Integration of Audiovisual Danger Stimuli in the Zebrafish Tectum is Linked with Premotor and Behavioral Enhancements

Nicolás Martorell[1] and Violeta Medan[1, 2]

[1] Instituto de Fisiología, Biología Molecular y Neurociencias (IFIBYNE) CONICET, [2] Departamento de Fisiología, Biología Molecular y Celular "Dr. Héctor Maldonado", Facultad de Ciencias Exactas y Naturales, Universidad de Buenos Aires, Ciudad Universitaria, (C1428EGA), Ciudad Autónoma de Buenos Aires, Argentina.

Abstract

Multisensory integration allows animals to combine cues from different sensory modalities to improve threat detection and drive evasive behaviors. While the zebrafish Tectum is classically viewed as a visual processing center, its role in integrating auditory and visual danger signals remains unclear. Using in vivo calcium imaging in larval zebrafish, we find that brief, high-amplitude auditory stimuli recruit a significant population of tectal neurons, predominantly in deep tectal layers. In addition, combined auditory and visual stimulation robustly increases both neural activity in the zebrafish Tectum and the probability of executing rapid escape maneuvers, especially for low salient stimuli. Interestingly, simultaneous auditory and visual cues engage more tectal neurons than either modality alone. Single neuron analysis reveal a population of neurons that respond to both auditory and visual cues, and importantly, shows that a proportion of those neurons only responds to multisensory stimulation. These results firmly establish the zebrafish Tectum as a multisensory processing area. Notably, the heightened tectal response during multisensory stimulation is strongly correlated with increased activity in hindbrain neurons implicated in escape-like motion events. These results link tectal multisensory integration to premotor circuits that drive behavioral output. Overall, our findings reveal the zebrafish Tectum as a hub for integration os audiovisual threat signals, and suggest a role of tectal multisensory processing in enhancing behavioral escape responses.

Introduction

Multisensory integration is a neural process by which animals combine information from different sensory modalities to build a coherent representation of their environment (Stein & Stanford, 2008; Van Atteveldt et al., 2014). This capability is essential for reducing ambiguity of sensory inputs, such as visual, auditory, and tactile cues, enhancing an organism's ability to detect and react to critical stimuli, such as predators, prey, or environmental hazards (Martorell & Medan, 2022; Lukas et al., 2021; Ohyama et al., 2015; McIntyre & Preuss, 2019).

This adaptive process has been widely documented across various animal species and contexts (Macaluso & Driver, 2005; Olcese et al., 2013; Whitchurch & Takahashi, 2006; Ghosh et al., 2017). In the mammalian superior colliculus, neurons integrate multisensory stimuli due to synaptic convergence of afferents conveying information from different sensory modalities (Meredith & Stein, 1986). Early studies in cats established that the neural response to multisensory stimulation can be supralinear with respect to the sum of the unisensory responses, and that integration effects are larger when weak or ambiguous stimuli are combined (Wallace et al., 1993; Stanford et al., 2005).

In other vertebrates, the Tectum, a structure homologous to the superior colliculus, is known to receive inputs from multiple sensory modalities (Isa et al., 2021; Knudsen, 1982; Hiramoto & Cline, 2009; Luksch, 2009; Hartline et al., 1978). This brain region is organized into distinct layers, primarily the neuropil –which receives afferents from retinal and other structures- and the periventricular layer (PVL) –composed of tectal somata- (Sajovic & Levinthal, 1982; Knudsen, 1982; Luksch, 2009). Retinotopic inputs of the visual field are received in the superficial layers of the neuropil, while deeper layers receive inputs from additional sensory modalities, like auditory, somatosensory and lateral-line inputs (Luksch, 2009). Neurons in the PVL are known to project to downstream targets in the hindbrain and spinal cord, where premotor neurons are involved in selecting and executing motor responses (Scott & Baier, 2009; Nevin et al., 2010). Despite receiving inputs from multiple sensory modalities and projecting to downstream motor centers, it is still unknown if the Tectum performs multisensory integration and if that integration influences motor output.

The Tectum of zebrafish (*Danio rerio*) has been traditionally associated with visual processing (Baier & Scott, 2024; Del Bene et al., 2010). While a few studies showed that tectal neurons can respond to non-visual stimuli such as auditory and water flow cues, responses were weak and sparse (Thompson et al., 2016; Vanwalleghem et al., 2017; Poulsen et al., 2021). One study reported multisensory suppression in some tectal neurons (Del Bene et al., 2010). However, no reports of robust multisensory enhancement in the zebrafish Tectum have been reported. Furthermore, it is not known whether tectal integration, if present, plays a functional role in influencing behavioral outputs.

A suitable model for studying audiovisual integration, zebrafish are vision and hearing specialists (Baier & Scott, 2024; Vanwalleghem et al., 2017; Fleisch & Neuhauss, 2006) with a well-documented behavioral repertoire (Kalueff et al., 2013; Marques et al., 2018). Specifically, danger stimuli evoke rapid escape responses known as C-starts, which allow fish to evade potential threats with remarkable speed and precision (Foreman & Eaton, 1993). Two types of fast escapes have received considerable attention due to their distinctive motor pattern and identifiable neural basis. The fastest escapes are short-latency C-starts (SLC), which are mediated by a pair of hindbrain premotor neurons, the Mauthner cells. Long-latency C-starts (LLC) are slower than SLC and mediated by Mauthner cell homologs and other hindbrain circuits (Burgess & Granato, 2007; Liu & Fetcho, 1999; Kohashi & Oda, 2008; Bhattacharyya et al., 2017; Marquart et al., 2019). These decision-making neurons, located in the hindbrain, receive sensory inputs from different structures, including the Tectum (Medan & Preuss, 2014; Zottoli et al., 1987; Preuss et al., 2006). Furthermore, SLC and LLC responses are known to be triggered by visual (e.g., looming objects) and auditory cues (e.g. abrupt sounds) (Temizer et al., 2015; Dunn et al., 2016; Kimmel et al., 1974).

In this study, we investigate whether audiovisual integration occurs within the Tectum and characterize its effects on behavioral decision-making in larval zebrafish. Through behavioral essays and calcium imaging at single-cell resolution we describe a strong multisensory enhancement of neural activation in the Tectum and of C-start probability during behavior. We observe robust auditory responses in the deep layers of the Tectum, consistent with observations in other vertebrate species. Moreover, we find that tectal integration exhibits classic features of multisensory processing, such as neurons with supralinear responses, and inverse effectiveness of integration with respect to the salience of unisensory stimuli.

Our findings reveal that tectal neurons respond more consistently when audiovisual stimuli converge. Crucially, we find that tectal multisensory enhancement is strongly correlated with the activation of premotor neurons in the hindbrain, suggesting that the zebrafish Tectum is a key site for multisensory integration and behavior selection.

Methods

Animal husbandry

We used larval zebrafish (*Danio rerio*) for this study. All animals were group-housed in 5 l aquaria of recirculating water, in a 14-10 h light–dark cycle (lights on at 8 am) in a temperature controlled room at 24-26 °C. All experiments were conducted between 9 am and 5 pm. Embryos were raised in E3 medium (5mM NaCl, 0.17 mM KCl, 0.33 mM CaCl2, 0.33 mM MgSO4) buffered with 10 mM HEPES (pH 7.3) at 28 °C, with medium changes every day. Larvae were fed AP100 (Zeigler Larval AP100 Diet) daily from 7 days post-fertilization (dpf) onward. We utilized 68 larvae aged 4 to 7 dpf of the line Nacre(elav3:GCaMP6f) for calcium imaging experiments. For behavioral experiments, we employed 80 wild type AB larvae aged 4 to 15 dpf. All experimental procedures were conducted in compliance with current regulations and were approved by the Institutional Animal Care and Use Committee of the Exact and Natural Sciences School, University of Buenos Aires (protocol 152).

Behavioral Experiments Setup

Behavioral assays were conducted in an arena consisting of a translucent plastic weighing boat of flat bottom, measuring 40 x 40 x 7 mm. The arena was filled with buffered E3 medium and was transilluminated using an infrared LED grid (55 x 55 mm, 36 LED units) and passed through opal diffusion glass to achieve more uniform irradiance. An overhead high-speed monochrome camera (720 x 540 px, 437 fps, Blackfly BFS-U3-04S2M-CS, FLIR) equipped with a 35 mm objective (59872, Edmund Optics) recorded larval behavior. The behavioral setup was mounted on an anti-vibration table and enclosed with opaque curtains to avoid unintended stimulation (Fig. 1A).

Calcium Imaging Experiments Setup

For calcium imaging experiments larvae were immobilized by complete embedding in 4% ultrapure low-melting agarose (A9414-25G, Sigma) and submersed in E3 medium. Calcium imaging was performed using

a Zeiss LSM-900 confocal microscope equipped with a 20× water-immersion objective lens (Zeiss W N-ACHROPLAN 420957). GCaMP6f was excited using a 488 nm laser, and emission was collected through a 509 nm dichroic mirror and 490-620 nm emission filter using a GaASP-PMT detector. For each larva, we acquired a z-stack encompassing the whole volume of both Tecta and adjacent structures (317 x 317 µm, 101 planes, interplane interval of 3 µm) to align brain images with the Z-Brain Atlas (Randlett et al., 2015) and a higher-resolution reference image used for ROI segmentation. We selected two planes of the brain along the dorsoventral axis to acquire (at 4.3 Hz), sequentially, the neural activity in response to sensory stimulus presentation.

Stimulus Presentation

Visual Stimuli

Visual stimuli were delivered using a 1.5-inch OLED display module (Waveshare) connected to an Arduino Due microcontroller. The display presented a looming stimulus (Adafruit_SSD1327 and custom C++ code) consisting of a dark circle that expanded over a white background. The looming stimulus had an l/v ratio of 1, where l is the radius of the virtual object and v is the approach speed (Gabbiani et al., 2002). The expansion phase lasted 25 s, followed by a 10-s period where the circle remained at its maximum size (Supp. Fig. 1A).

As multisensory enhancement depends on stimulus salience (Martorell & Medan, 2022), we designed stimuli of varying intensity. To change the intensity of the visual stimulus, we adjusted the contrast of the expanding circle against a constant white background. The contrast is expressed as:

$$\textit{Michelson Contrast (MC)} = (I_{background} - I_{disk}) / (I_{background} + I_{disk})$$

where $I_{background}$ is the irradiance of the background (33 mW/m²) and I_{disk} is the irradiance of the dark disk. The irradiance was measured using a Tektronix J17 photometer equipped with a J1812 sensor. Based on preliminary experiments we defined three levels of visual contrast (Fig. 1B): V_{min} (MC = 0.13), V_{med} (MC = 0.29), V_{max} (MC = 0.59) which showed progressive increase in the probability of eliciting an escape response (Fig. 1D).

Auditory Stimuli

Auditory stimuli were produced by a speaker (Thonet & Vander HK096-03451). The speaker was placed on foam insulation padding and positioned at 10 cm from the arena. The intensity of the auditory stimuli was measured on air using a sound level meter (Yu Fung Model YF-20) and reported in decibels (dB re. 20 µPa).

The speaker emitted a single-cycle sine wave at 220 Hz generated and transmitted directly from the sound card of the stimulation computer. To modulate the intensity of the auditory stimuli, we varied the amplitude of the sine wave, defining three levels (Fig. 1B): A_{min} (60 dB), A_{med} (69 dB), A_{max} (75 dB) which had respectively low, medium and high salience in terms of the probability of eliciting an escape response

(Fig. 1D). Visual and auditory stimuli were triggered and synchronized using a custom script written in Processing (Processing Foundation).

Multisensory Stimuli

We combined the 3 visual and 3 auditory unisensory stimuli to create 9 multisensory stimuli (Fig. 1B). In multisensory stimuli, the auditory stimulus was timed to coincide with the end of the looming visual stimulus, simulating the simultaneous arrival of visual and auditory cues indicative of an approaching threat (Supp. Fig. 1A). Previous work from our lab showed that this stimulus configuration effectively evokes escape responses in fish (Martorell & Medan, 2022). Visual and auditory stimuli were presented from sources located at 90° (behavioral experiments, Fig. 1A) or 135° (calcium imaging experiments, Supp. Fig. 1B) from each other. Preliminary experiments showed that the auditory stimulus does not have a strong directional component in our conditions. For imaging experiments, we used only tested responses to V_{min}, V_{max} and A_{max} and their combinations.

Experimental Procedures

Prior to the start of experiments, larvae were given at least 6 minutes to acclimate to the experimental setup. In behavioral experiments individual larvae were exposed to each of the uni- or multisensory stimuli once, and an additional control condition with no stimulation in random order totaling 16 trials with an intertrial interval (ITI) of 40 s (Fig. 1B, Supp. Fig. 1A). In calcium imaging experiments, larvae were exposed to 5 repetitions of a subset of these conditions: V_{max}, A_{max}, their multisensory combination and the control condition (random order, 20 trials in total). Some calcium imaging experiments (Fig. 4) also included the V_{min} in combination with A_{max} (30 trials in total, ITI = 40 s).

Behavioral Data Analysis

Pose Estimation Using DeepLabCut and Behavioral Event Classification

Larval motor behavior was tracked using DeepLabCut (Mathis et al., 2018). We trained a ResNet-50 convolutional neural network where the output layer was replaced with a pose estimation layer designed to predict the location of 12 anatomical landmarks as scoremap grids: one point for each eye, two points for the swim bladder, and eight points along the tail. Training was performed on a single NVIDIA GeForce RTX 3060 GPU with 12 GB of VRAM.

An initial training dataset was created by annotating 152 frames from a library of 1,280 behavioral recordings. Frames were chosen to maximize variability in body poses, positions within the arena, fish sizes, and lighting conditions. For a second training iteration, we annotated an additional 125 frames where the model's initial predictions had low likelihood scores (high uncertainty in model predictions).

The annotated dataset was split into training and validation sets, with 95% of the images used for training and the remaining 5% reserved for model evaluation. Using pose estimation data we calculated 36 kinematic parameters, such as linear head velocity or total body curvature (Supp. Table 1). Discrete activity events, or bouts, were identified by detecting peaks in the linear head velocity time series. Events exceeding a threshold of 6 cm/s were classified as fast responses, as visual inspection of video recordings showed that all events exceeding this threshold were C-starts. (Fig. 1C).

184

185 ***Quantification of Multisensory Integration***

186 I0n both behavioral and imaging experiments, multisensory integration was quantified by comparing the
187 activity elicited during multisensory stimulation with the activity observed during the most effective
188 unisensory stimulus (Stevenson et al., 2014). For behavioral experiments, activity was measured as the
189 probability of eliciting a fast response, while in imaging experiments, it was measured as the proportion
190 of active ROIs.

191 The multisensory integration coefficient (MI) was calculated using the formula:

192 $$MI = (P_{multi} - P_{max\ uni}) / (P_{multi} + P_{max\ uni})$$

193 where P_{multi} represents the activity during the multisensory stimulus, and $P_{max\ uni}$ represents the activity
194 during the unisensory stimulus that elicited the largest response. An MI value of zero indicates no effect
195 of multisensory integration beyond the maximum unisensory response. A negative MI value indicates
196 multisensory suppression, whereas a positive MI value indicates multisensory enhancement.

197

198 **Calcium Imaging Data Processing and Analysis**

199 ***Image Registration, Motion Correction and Cell Segmentation***

200 Calcium imaging recordings were processed to correct for motion artifacts and registered to the higher-
201 quality template using the CaImAn library (Giovannucci et al., 2019). We next used custom Python code
202 for semi-automated Region Of Interest (ROI) detection based on the anatomical features of the images.
203 Note that the calcium sensor expression is cytosolic and therefore cell nuclei are not fluorescent. The
204 Tectum is organized into the PVL, a deep layer containing most neuronal somas, and the neuropil, a
205 superficial layer where dendrites and afferent axons converge. We detected ROIs in three specific brain
206 regions of interest: the tectal neuropil, the periventricular layer of the Tectum (PVL), and the hindbrain
207 (Supp. Fig. 1C). To estimate the proportion of the visible neuropil area exhibiting significant activity we
208 analyzed the neuropil both as an entire undivided region and by subdividing it into a grid 5 µm x 5 µm to
209 capture regional changes in neurite activity.

210 ***Fluorescence Normalization and Time Series Analysis***

211 For each ROI we calculated fluorescence time series by averaging the pixel intensities within the ROI for
212 each recorded frame. These time series were then normalized to ΔF/F, defined as:

213 $$\Delta F/F = (F - F_0) / F_0$$

214 where F is the fluorescence intensity at a given time point, and F_0 is the baseline fluorescence (example
215 shown in Supp. Fig. 1Di). The baseline F_0 was calculated as the 8th percentile of a 60-frame (approx. 14 s)
216 window preceding the current frame. We next binarized the ΔF/F time series for each ROI and set a
217 threshold of 1.2 SD above the mean ΔF/F value. Any ΔF/F value exceeding this threshold was considered
218 an event of activation at that frame (example shown in Supp. Fig. 1Dii). ROIs inactive during the entire

recording session were excluded from subsequent analysis. All experiments had ROIs responding to visual stimuli, however we only included experiments where at least one ROI responded in at least 3 out of 5 auditory trials (33 planes from 24 animals, out of 113 planes from 68 animals). Responses were quantified in a 2.8 s (12 frames) window after stimulus presentation (Supp. Fig. 1D, magenta shaded area). ROIs were classified as responsive if they exhibited activity in at least one of the five trials of that stimulus during the stimulation window. The consistency of a ROI's response was quantified by counting the number of trials in which the ROI was active during the stimulation window (i.e. the consistency values ranged 0 to 5).

To examine population-level neural representations, we performed temporal principal component analysis (t-PCA) on ΔF/F time series from PVL neurons (Supp. Fig. 2). The analysis was restricted to a window following stimulus onset, which encompassed the peak of population responses. This dimensionality reduction allowed us to project N-dimensional neural activity patterns (where N is the number of PVL neurons recorded in each experiment) onto a two-dimensional space, facilitating the visualization and comparison of population trajectories across sensory conditions.

Identification of Motion-Correlated Neurons

Although embedded in agarose, larvae showed clear motor responses reflected as time-locked displacements of the image in the frames immediately following sensory stimuli. The frame-by-frame displacement data obtained from motion correction analysis were used to construct a continuous estimate of the animal's movement over time (Supp. Fig. 1E). To detect candidate motor events, we calculated the mean displacement for each experiment, averaged over all recorded frames. Any frame where the displacement exceeded 4 SD above the experiment's mean displacement was considered a motion event. This threshold captured large, abrupt displacements indicative of motor-related activity while minimizing the influence of minor shifts that could result from slight image drift.

Statistical Analysis

All statistical analyses were conducted using Python (v3.9) with the SciPy and Statsmodels libraries. Statistical significance was assessed at a threshold of $\alpha = 0.05$. Binomial Generalized Linear Models (GLMs) were used to evaluate the effects of visual and auditory stimuli on escape response probabilities. Mixed effect models were used in some cases to factor in the variance accounted for by individual differences. Model significance was tested using likelihood ratio tests, and parameter estimates are reported with their associated p-values. The significance of MI values across conditions was assessed using one-sample t-tests. Wilcoxon Signed-Rank Tests were used to compare paired conditions in imaging experiments (e.g., auditory vs. control, multisensory vs. visual), while non-paired tests were performed using Mann-Whitney U-tests. Z-Tests for Regression Slopes were used to compare slopes between different conditions. All analyses were corrected for multiple comparisons where applicable using the Holm-Bonferroni method. Error bars represent standard error unless otherwise specified. Graphs and visualizations were generated using Matplotlib and Seaborn libraries. The code is open-source and available in GitHub.

Results

Multisensory Stimulation Enhances Escape Probability in Freely-Swimming Fish

To determine how multisensory information influences escape behaviors, we conducted behavioral experiments in 40 4-7 dpf freely swimming zebrafish (Fig. 1A). Visual and auditory stimuli of different intensities were presented individually and in combination, including three levels of visual contrast, three levels of auditory amplitude, and their nine combinations, along with a no-stimulus control (Fig. 1B). High-speed video recordings of locomotor activity were used to train a deep learning model for pose estimation, which allowed us to track and extract precise kinematic data. Fast escape behaviors were identified as rapid movements exceeding a head velocity threshold of 6 cm/s (Fig. 1C). By analyzing the probability of eliciting an escape response, we evaluated how different sensory modalities and their combinations affected escape behavior.

The probability of eliciting a fast escape response increased with the intensity of both visual and auditory stimuli (Fig. 1D; Mixed Effects Binomial GLM, fish identity as a random effect, auditory effect: 0.91, $p<0.0001$; visual effect: 0.46, $p<0.0001$). To quantify the effect of combining sensory modalities, we calculated a multisensory integration coefficient (MI) for each of the nine audiovisual conditions. The MI compares the escape probability during multisensory stimulation to the most effective unisensory stimulus (see Methods). This analysis revealed that combined audiovisual stimuli significantly increased escape probabilities beyond the maximum unisensory response (Fig. 1E; the mean of the MI values for all multisensory conditions is significantly greater than 0, Wilcoxon Signed-Rank Test, $p = 0.037$). Interestingly, the magnitude of this enhancement was inversely related to the intensity of the auditory stimulus (Gaussian GLM, auditory effect: -0.115, $p = 0.009$) while the intensity of the visual stimulus had no significant impact on the MI (visual effect: -0.006, $p = 0.90$). This was further supported by the negative correlation between the MI of each audiovisual condition and its maximum unisensory response probability (Fig. 1F, Linear Regression, slope = -0.50, $p = 0.013$, $R^2=0.61$). These findings agree with the principle of inverse effectiveness, where weaker unisensory stimuli produce proportionally greater multisensory enhancements (Stein et al., 2009; Rowland et al., 2007). For instance, the weakest auditory stimulus (60 dB), elicited responses in 15% of trials while the lowest contrast visual stimulus (Michelson Contrast 0.13) elicited responses in 10% of the trials. When these two weak stimuli were combined (stim. 7 in Fig. 1B), the response probability rose to 33% (Fig. 1D), yielding a multisensory integration coefficient of 0.37 (Fig. 1E-F). In contrast, responses evoked by the strongest auditory stimulus (75 dB) did not show multisensory enhancement, showing almost no change compared to its unisensory response probability (Stims. 3, 6 and 9 in Fig. 1F).

Overall, these results confirm that zebrafish can combine audiovisual information to decide whether to execute a fast escape response (Martorell & Medan, 2022), and that the strongest multisensory enhancement is produced by exposure to the weakest stimuli.

Auditory Stimulation Elicits Neural Responses in the Tectum

293 Larval zebrafish are capable of integrating multisensory information during fast escapes (Fig. 1). We thus
294 investigated audiovisual representation within the Tectum. While visual processing in the fish Tectum has
295 been described, accounts of auditory coding are scarce and focused on the representation of pure tones
296 (Thompson et al., 2016; Vanwalleghem, Heap, & Scott, 2017; Privat et al., 2019; Poulsen et al., 2021). Here
297 we used a brief and abrupt sound which can evoke fear responses (Fig. 1) to ask whether this classically
298 visual brain region also responds to auditory danger stimuli.

299 To answer this question, we performed *in vivo* confocal calcium imaging in agarose embedded larval
300 zebrafish at 4-7 dpf expressing the cytoplasmic calcium indicator GCaMP6f (Nacre(elav3:GCaMP6f))
301 (Supp. Fig. 1B). We imaged the PVL and the tectal neuropil during the presentation of auditory and visual
302 stimuli (Supp. Fig. 1C) and quantified the tectal response during a trial as the proportion of active ROIs
303 during a 2.8 s window after sound presentation (Fig. 2).

304 We found that the presentation of an auditory stimulus produced a robust response in the PVL (Fig. 2A)
305 whereas the number of spontaneously active neurons in this region was relatively low (control trials, Fig.
306 2B). Across 33 experiments (13851 ROIs), the mean proportion of active ROIs activated by auditory
307 stimulation showed a sharp increase after onset of stimulation (dashed vertical line Fig. 2A) while control
308 trials showed a steady and low proportion of spontaneously active ROIs. Auditory stimulation produced a
309 peak synchronic activation of around 8% of PVL neurons (Fig. 2C), a proportion notably higher than the
310 basal 3% observed in control trials. The mean proportion of active neurons for auditory trials was also
311 significantly higher than for control trials (Fig. 2D, median: Ctrl = 2.7%, Aud = 8.9%; Wilcoxon signed-rank
312 test, $p < 0.001$).

313 The auditory-evoked neural representation in the PVL displays a consistent pattern across trials of the
314 same animal. Figure 2E shows a representative example of auditory responsive neurons in the PVL.
315 Neurons that were active following auditory (blue dots, Fig. 2E) or control (black dots, Fig. 2F) stimulation
316 are highlighted. Auditory responsive neurons could be randomly scattered in the tectum or show some
317 kind of topographical assembly. To test this, we measured the compactness of the auditory response as
318 the mean nearest-neighbor distance among auditory-responsive ROIs. Taking the ratio of compactness of
319 auditory neurons and a random subset of ROIs reveals that auditory-evoked representations are more
320 compact than expected by chance (median: Aud: 0.12, Ctrl: 0.09; compactness ratio is significantly greater
321 than 1; Wilcoxon signed-rank test, $p < 0.001$). This indicates a non-random clustering of responsive
322 neurons which was, however, variable from animal to animal.

323 The tectal neuropil also showed robust auditory responses (Fig. 2G). To quantify those responses, we
324 subdivided the neuropil into a grid of ROIs given the absence of clearly identifiable somas. Neuropil ROIs
325 had approximately the same area as ROIs defined in the PVL, however, contrary to PVL ROIs, neuropil ROIs
326 do not correspond to somata but quantify the fluorescence emitted by the neurites located within.

327 Responses in the tectal neuropil during auditory trials (Fig. G, K) were stronger and more synchronous
328 than during control trials (Fig. 2H, L). Auditory stimulation produced a bilateral and synchronized activity
329 of grid ROIs which clustered towards the medial edge of the tectal neuropil (Fig. 2K) while in control trials
330 only a few, scattered grid ROIs were active (Fig. 2L). Fig. 2I shows the dynamics of neuropil activation,
331 which reaches on average 13% of the total neuropile area which was significantly higher for auditory than

for control conditions (Fig. 2J; median: Ctrl = 2.9%, Aud = 7.3%; Wilcoxon signed-rank test, $p < 0.001$). These findings show that, as the PVL, the neuropil exhibits a clear auditory response.

These results show that the neuropil's response to auditory stimulation was concentrated in deeper layers (Fig. 2K) while activity in the superficial layers was rarely observed. We quantified this by computing the mean distance of the activated neuropil ROIs to the medial edge of the Tectum (green line in Fig. 2K) and found that this distance was significantly smaller than that of a null model created by randomly selecting the same number of ROIs (mean +/- sd: 26.78 ± 10.18 µm vs. 30.56 ± 7.19 µm; Wilcoxon signed-rank test, $p = 0.002$), indicating a non-random clustering of responsive neurons

Auditory Inputs Enhance Visual Coding in the Tectum

The Tectum participates in the processing of visual looming stimuli (Barker & Baier, 2015; Marquez-Legorreta, Piber, & Scott, 2020). Here we investigated whether auditory cues presented concurrently with a visual looming stimulus (Supp. Fig. 1A-B) could enhance tectal activity (Fig. 3).

In the PVL, the responses during multisensory trials recruited a larger number of neurons across experiments compared to visual stimuli alone. Visual trials elicited clear responses that recruited a significant proportion of PVL neurons (Fig. 3A), but multisensory trials induced larger and synchronic activation immediately following the auditory stimulus onset (Fig. 3B-C). Across experiments, the recruitment of ROIs reached a higher peak in multisensory trials, the mean proportion of active ROIs in the PVL (shaded area in Fig. 3C) was significantly larger than in visual activation alone trials (Fig. 3D, median: Vis = 13.0%, Multi = 20.7%; Wilcoxon signed-rank test, $p < 0.001$). These results indicate that combining an auditory and a visual cue can significantly increase neuronal recruitment in the PVL. The visual stimulus was delivered from the left side of the animal producing a visual response principally in the contralateral (right) hemitectum (Fig. 3E). Surprisingly, the same visual loom paired with an auditory stimulus recruited a comparable proportion of ROIs in both hemispheres (Fig. 3F).

We next asked if multisensory enhancement could be detected in the neuropil as well, and how the anatomical representation of the responses would relate to the visual representation. We observed a robust increase in the proportion of active neuropil area during multisensory trials compared to visual trials (Fig. 3G vs. 3H). The peak proportion of active grid ROIs during multisensory stimulation was 10% higher than in visual only trials (Fig. 3I) while the mean proportion of active neuropil area was 5% higher in multisensory trials compared to visual trials (Fig. 3J, Vis = 19.3%, Multi = 25.4%; Wilcoxon signed-rank test, $p < 0.001$). Notably, the addition of the auditory stimulus caused the activation of deeper layers of the visible part of the ipsilateral neuropil (ROIs closer to the medial edge, green curves, Fig. 3L), just like we observed with the unisensory auditory stimulus (Fig. 2K). Indeed, the mean distance of the activated neuropil regions to the medial edge was lower in multisensory trials compared to visual trials (Fig. 3K-L, visual, mean +/- sd: 29 +/- 7 um vs. multisensory: 27 +/- 8 um; Wilcoxon signed-rank test, $p = 0.0014$). These results suggests that the neuropil's response to audiovisual stimulation is a combination of visually-evoked activity in superficial layers and auditory-evoked activity in deeper layers, likely serving as the multisensory inputs subsequently processed by the PVL.

Multisensory Enhancement of Tectal Response Shows Inverse Effectiveness with Stimulus Salience

Numerous studies have reported that the multisensory enhancement of neural responses tends to be inversely related to the effectiveness of the inputs when received separately (Meredith & Stein, 1986; Stein et al., 2008; Gil-Guevara, Bernal, & Riveros, 2022; Sumby & Pollack, 1954, Martorell & Medan, 2022) and thus, particularly effective when individual signals are weak or ambiguous. To ask if multisensory integration in the Tectum also shows inverse effectiveness, we presented the auditory cue (A_{max}, Fig. 1B) in combination with a low-contrast visual loom (V_{min}. Fig. 4A) or a high contrast loom (V_{max}, Fig. 4C) and tested if decreasing the intensity of the visual stimulus increased multisensory enhancement in the zebrafish Tectum.

While low-contrast visual stimulus (V_{min}) evoked a tectal response in 1.5% of PVL neurons (median, light red box, Fig. 4B), V_{max} recruited 10.2 of PVL neurons (red box, Fig. 4D), a significantly higher proportion (V_{min} vs. V_{max}, Wilcoxon signed-rank test, $p < 0.001$). However, we observed an increase in the mean % of active ROIs both with V_{min} combined with an auditory stimulus (Fig. 4B, V_{min}= 1.5% vs. AV_{min}= 4.7%; Wilcoxon signed-rank test, $p = 0.004$) and with V_{max} combined with an auditory stimulus (Fig. 4D, V_{max}= 10.2% vs. AV_{max}= 15.5%; Wilcoxon signed-rank test, V_{max} vs. AV_{max}, $p < 0.001$). The MI (Multisensory Index, see Methods) was MI_{min}= 0.25 for the low-contrast multisensory stimulus and MI_{max}= 0.14 for the high-contrast multisensory stimulus. This larger multisensory enhancement for the low-contrast condition than for the high-contrast condition suggests that in the tectal PVL the multisensory integration shows inverse effectiveness.

In the neuropil (Fig. 4E-H) we observed a similar relationship between visual contrast and the proportion of active neuropile area (light red vs. red traces, Fig. 4E and G) or the mean % of active neuropile area (light or red boxes in Figs. F and H, V_{min}= 6.5% vs. V_{max}= 26.3%–). The effect of combining a visual and an auditory stimulus was stronger for V_{min} (Fig. 4F; V_{min}= 6.5% vs. AV_{min}= 13.1%; Wilcoxon signed-rank test, $p = 0.001$, $MI_{min} = 0.22$) but there was also a significant enhancement for the high-contrast condition (Fig. 4H, V_{max}= 26.2% vs. AV_{max}= 32.1%; Wilcoxon signed-rank test, $p < 0.001$, $MI_{max} = 0.08$).

The effective salience of a visual stimulus is not only a function of its contrast, but also depends on gaze direction, attentional state and other factors that can vary between animals. We thus analyzed, for each individual experiment (larvae) the relationship between the MI and activity during the visual unisensory condition in the PVL (Fig. 4I) and in the neuropil (Fig. 4J). The inverse effectiveness hypothesis predicts that in experiments where the visual stimulus evokes a weaker response there will be a stronger multisensory enhancement. Indeed, MI and the maximal unisensory response are inversely related for both conditions using a single exponential-decay model, both in the PVL (Fig. 4I; exponential fit, b>0, two-sided $p = 0.0013$, $R^2 = 0.571$, $n = 58$) and in the neuropil (Fig. 4J; exponential fit, b>0, two-sided $p = 0.00070$, $R^2 = 0.589$, $n = 54$). Low-contrast stimuli are usually perceived as less salient and therefore tend to produce higher MI values compared to the high-contrast condition (purple vs. magenta dots in Figs. 4I and J), although this difference is not significant in the PVL (Wilcoxon signed-rank test, paired by experiment, $p = 0.20$), possibly due to variability across animals. In the neuropil, however, MI values for the low-contrast condition are significantly higher than for the high-contrast condition (Wilcoxon signed-rank test, paired

409 by experiment, p = 0.019). Overall, this shows that the Tectum exhibits stronger multisensory
410 enhancement when the unisensory components of the multimodal stimulus have lower salience, a
411 hallmark of multisensory integration.

412

413 **Multisensory Stimulation Recruits Unresponsive PVL Neurons and Boosts Response Probability of**
414 **Audiovisual Neurons**

415 While the zebrafish Tectum shows multisensory enhancement at the population level (Fig. 3) and this
416 effect alone could have important consequences on downstream circuits, actual multisensory integration
417 in tectal units requires that individual neurons change their response when auditory and visual cues are
418 combined. This is because an increase in the proportion of active neurons could be due to a sum of
419 independent unisensory responses occurring in distinct units, and not to true multisensory integration at
420 neuronal level. We thus asked if this multisensory enhancement would also be observable at the individual
421 neuron level, which in our experiments, should be reflected in units that are only active when auditory
422 and visual inputs are simultaneously present.

423 We analyzed the response profiles to unisensory and multisensory stimuli of individual PVL neurons from
424 24 animals. Based only on their response to unisensory stimuli (i.e. excluding multisensory trials) we
425 categorized PVL neurons in four distinct classes: neurons that responded only to auditory stimulation,
426 neurons that responded only to visual stimulation, neurons that responded to both modalities (i.e. to
427 unisensory auditory or unisensory visual stimuli), and neurons that did not respond to either unisensory
428 auditory or unisensory visual stimuli. This last group was further divided into two classes depending on
429 whether neurons were (only) responsive to multisensory stimulation or unresponsive to all stimulation.
430 It's important to point out that, although auditory stimulation produced bilateral activation of the Tectum
431 (see examples on Figs. 2E, K), visual stimulation produced preferential activation of the hemitectum
432 contralateral to the screen (Fig. 3E, K). We thus restricted the analysis to the contralateral Tectum (left
433 Tectum, Supp. Fig. 1B), where activation of both visual and auditory inputs was robust.

434 A representative example of this distribution is illustrated in Fig. 5A, where ROIs are color-coded based
435 on the neuron response profile. The spatial distribution and proportions of these neuron types varied
436 across experiments, and we did not find any indication of spatial clustering of the responses (other than
437 retinotopy for stimuli with a visual component). On average, 21% of PVL neurons were unresponsive to
438 all stimuli (Fig. 5B, U, grey bar). 29% of PVL neurons were responsive to visual looms but never to auditory
439 stimuli (Fig. 5B, EV, yellow bar) while 19% showed the opposite, being only responsive to auditory stimuli
440 (Fig. 5B, EA, blue bar). To confirm that these neurons were truly insensitive to their non-preferred
441 modality in our stimulation conditions, we compared their activity during its preferred-modality
442 stimulation against their activity during multisensory trials. Neither of the two populations showed an
443 increased response to multisensory stimulation (EA, Wilcoxon signed-rank test, p = 0.12; EV, Wilcoxon
444 signed-rank test, p = 0.89, not shown). This could be explained because of the nature of our stimuli and/or
445 the spatial configuration of our setup not being effective (e.g. retinotopic effects for the visual stimulus
446 and possible dependence on sound features for the auditory stimulus), but it could also point to some PVL
447 neurons truly receiving only one kind of sensory input.

448 On average 19% of PVL neurons responded to the visual loom but also to unisensory auditory trials (Fig.
449 5B, AV, light-green bar), a proportion much larger than the <1% previously reported for non-danger
450 audiovisual cues (Thompson et al., 2016). We asked if these AV neurons that are activated by both
451 unisensory auditory and unisensory visual stimuli would increase their responsiveness when presented
452 with those stimuli simultaneously, or if they would show audiovisual suppression as previously shown for
453 non-danger cues (Thompson et al., 2016). To answer this, we quantified the consistency of each AV neuron
454 as the number of trials in which it was active for a particular stimulus. This value can range from 0 (for a
455 consistently inactive ROI) to 5 (for a ROI that was activated on each of the 5 trials for a particular
456 condition). We calculated the consistency of each AV neuron individually for each stimulation condition:
457 no stimulation (Ctrl), auditory (Aud), visual (Vis) and multisensory (Multi, Fig. 5C). Given that visual
458 responses were stronger and more consistent than auditory responses across our experiments, we
459 compared the multisensory consistency against the visual consistency and found that AV neurons
460 increased their consistency (i.e. their individual probability of response) for multisensory vs. visual trials
461 (Mixed Effects Linear Regression, fish identity as a random effect, effect size = 0.15, p = 0.04). This can
462 also be seen when calculating the proportion of active audiovisual ROIs over time (Fig. 5Di), where the
463 peak multisensory activity of these neurons is significantly higher than their peak activity for either of the
464 two unisensory stimuli (Fig. 5Dii, Wilcoxon signed-rank test, p = 0.012). These results parallel those
465 observed for the whole population of PVL neurons (Figs. 3D, 4B-F), critically, it shows that simultaneous
466 auditory and visual input can enhance response probability at the individual neuron level.

467 Strikingly, we found that about 13% of PVL neurons were silent during all ten unisensory trials but
468 responded to (at least once) multisensory stimulation (Fig. 5B, EM, dark-green bar). To ensure that these
469 responses were not due to spontaneous activity, we compared the activity of these neurons during
470 multisensory trials against their activity during control trials. EM neurons were more consistently active
471 during multisensory stimulation than in unisensory or control trials (Fig. 5E) and their peak response
472 probability was as well significantly higher when compared to control trials (Fig. 5F, Wilcoxon signed-rank
473 test, p < 0.001). This shows that multisensory stimulation can recruit units which, although receive inputs
474 from both modalities, are silent unless those inputs are activated simultaneously.

475 We next asked if the activity of AV neurons would form distinct representations of visual and auditory
476 stimuli (i.e. different responses to auditory and visual unisensory stimuli), and, if so, how multisensory
477 representations would relate to unisensory representations (Supp. Fig. 2). To answer this question, we
478 performed temporal principal component analysis (t-PCA) on the dF/F data from individual AV PVL
479 neurons during visual, auditory, and multisensory trials within a 1.8 second window after stimulation time
480 (which encompasses the period where populational responses reaches their peak, Fig. 5Di). This allowed
481 us to transform N-dimensional activation patterns (where N is the number of PVL neurons in a particular
482 experiment) into trajectories in 2D space which encode information about the temporal dynamic of the
483 tectal representation for each trial.

484 Two representative examples from two different animals are shown in Supp. Fig. 2A and B. Plots of the
485 first two components of the PCA show trajectories for trials that showed a significant response, i.e. there
486 can be up to 5 trajectories for each type of stimulus (lines correspond to PVL trajectories in response to
487 visual (red), auditory (blue) and multisensory (magenta) stimuli). All trajectories were normalized to start

488 at the origin, which represents the Tectum state before stimulation. Trajectories corresponding to visual
489 and auditory trials diverged in PCA space (median angle between visual and auditory trajectories was 60°),
490 suggesting that the tectal representation to visual and auditory stimuli are different.

491 To describe the variability of the multisensory patterns of activity and compare it to their unisensory
492 counterparts in all experiments, we calculated the median unisensory direction for each unisensory
493 stimulus (red and blue vectors in Supp. Fig. 2A and 2B) and evaluated the angle of each multisensory
494 trajectory with both unisensory vectors (Supp. Fig. 2C). Most multisensory patterns of activity align with
495 either the visual or the auditory representation, i.e. each pattern of activity has a small angle with the
496 visual vector and a larger one with the auditory vector or vice versa, with the visual mode being more
497 common (Supp. Fig. 2C, 73% visual, 27% auditory). To quantify the separation between unisensory
498 representations, we treated each complete trajectory (spanning 8 post-stimulus frames) as a single vector
499 in a 16-dimensional space (2 coordinates x 8 time points). We then computed the average Euclidean
500 distance between all pairs of visual-auditory trajectories (inter-modality distance) and compared it to the
501 average distances within the same modality (intra-modality distances, i.e., visual-visual and auditory-
502 auditory). As shown in Supp. Fig. 2D, the inter-modality distance was significantly greater than intra-
503 modality distances (Mann-Whitney U test, $p < 0.001$). This analysis confirms that visual and auditory
504 stimuli evoke distinct and separable population activity patterns in the PVL.

505 To determine whether the multisensory response aligned with one of the unisensory inputs or had a
506 distinct activity pattern, we compared the multisensory trajectories against their unisensory counterparts.
507 First, we computed the average Euclidean distance between multisensory and auditory trajectories (inter-
508 modality) and compared it to their respective intra-modality distances (Supp. Fig. 2E). The multisensory-
509 auditory distance (black dots) was significantly greater than both the intra-multisensory (magenta dots)
510 and intra-auditory (blue dots) distances (Mann-Whitney U test, $p < 0.001$). Conversely, when we
511 performed the same comparison between multisensory and visual trajectories (Supp. Fig. 2F), the inter-
512 modality distance (multisensory vs. visual, black dots) was not significantly different from the intra-
513 modality distances (magenta and red dots) (Mann-Whitney U test, $p = 0.12$). This analysis confirms that
514 the population response to the multisensory stimulus is closer to the visual-only response, as opposed to
515 the auditory-only response.

516

517 **Multisensory Integration in the Tectum Is Associated with Enhanced Motor Responses in the Hindbrain**

518 We have shown that the zebrafish Tectum integrates visual and auditory information, enhancing neural
519 responses. Does this multisensory enhancement have a functional behavioral value? The Tectum is known
520 to project to premotor regions in the hindbrain, both in zebrafish and in other vertebrate species (Del
521 Bene et al., 2010; Baier & Scott, 2024). Some hindbrain neurons receive input from the Tectum to evoke
522 fear-related responses, such as the Mauthner cell-initiated C-start responses (Zottoli et al., 1987; Zottoli,
523 1977; Zottoli et al., 1999). It is therefore possible that audiovisual integration in the Tectum could affect
524 premotor neurons and, consequently, influence the execution of behavioral responses. For this reason,
525 we next explored the relationship between the enhancement of tectal activity during multisensory trials
526 and behavioral output. Although larvae were agarose-embedded to restrict brain movement during image

527 acquisition they still exhibited small, sudden movements that were registered during the recording. These
528 sudden movements in the x-y plane are routinely corrected using a motion correction algorithm before
529 ROI extraction (Giovannucci et al., 2019). Interestingly, we noticed that these motion events were more
530 frequent during stimulus presentation. Frame-by-frame displacements of confocal images larger than 4
531 SD above the mean displacement of each experiment were considered to be motion events. Across all
532 analyzed experiments (n=33) we found that these motion events were more common within the period
533 following visual (4%) or auditory (6%) stimulation than during spontaneous activity (1%). Crucially, the
534 probability of eliciting motion events during multisensory trials (12%) was significantly higher than the
535 maximum unisensory (auditory) condition (Fig. 6A, Paired t-test, Aud vs. Multi, t= 2.26, p = 0.03). This
536 parallels the multisensory enhancement we observed for escape responses in behavioral experiments
537 (Fig. 1D-E), although response probabilities here are much lower, likely because of the differences in the
538 conditions of stimulus administration. If these events represent actual motor responses this should be
539 reflected in activity of hindbrain neurons. We focused on neurons primarily located in rhombomeres 1
540 and 2, which were imaged simultaneously with tectal activity. To identify candidate premotor neurons,
541 we first calculated the activation probability of each hindbrain neuron considering only spontaneous
542 motion events (i.e. events occurred in the absence of sensory stimulation). We next produced a shuffled
543 distribution, where motion event times were randomized to eliminate real correlations and compared the
544 real and shuffled distributions. We defined motion-correlated neurons (MCN) as those units with an
545 activation probability higher than 99th percentile of the shuffled distribution (Fig. 6B, green area).

546 We confirmed that this population of hindbrain neurons was active during both spontaneous and
547 stimulus-evoked motion events (Fig. 6C). Notably, the proportion of MCNs that became active in response
548 to sensory stimulation was higher for auditory than for visual trials and showed multisensory
549 enhancement over the auditory condition (Fig. 6D, Mann-Whitney U test, p = 0.037), reproducing the
550 pattern observed in the motion events (Fig. 6A).

551 The enhancement in the proportion of active MCN of the hindbrain after multisensory stimulation (Fig.
552 6D) was reminiscent of the multisensory enhancement we observed in the Tectum (Figs. 3B, 4B). We thus
553 asked if the level of activity of the MCNs correlated with MI observed in the Tectum. For each multisensory
554 trial, we calculated tectal MI, similarly to what we did in Fig. 4A-B to quantify multisensory enhancement
555 (see Methods). We observed that when tectal MI was zero or negative—indicating no enhancement or
556 suppression—the activation of MCN in the hindbrain was weak and not significantly associated with MI
557 (Fig. 6E, blue area; linear regression, $p = 0.716$). However, when tectal MI was positive, there was a strong
558 positive association between MI and MCN activity (Fig. 6E, green area; linear regression, $p < 0.001$,
559 coefficient = 0.65). This shows that there is a positive relationship between multisensory enhancement in
560 the Tectum and hindbrain activity linked to behavioral output. Crucially, this relationship is rectified as a
561 function of integration valence: only positive multisensory effects in the Tectum are associated with an
562 increased probability of MCN activation in the hindbrain.

563 To determine if this association between tectal MI and hindbrain activity was driven by all or by a subset
564 of MCNs, we calculated the mean dF/F of the five multisensory trials for each MCN and computed the
565 correlation coefficient between its mean dF/F and the tectal MI value for the corresponding trials (Tectal
566 M - corr. coef. MCN). This metric indicates, for each experiment, how strongly each MCN was correlated

567 with tectal MI during multisensory stimulation. In Fig. 6F black bars represent the real distribution of
568 Tectal M - corr. coef. MCN for an example experiment while gray bars show the results when shuffling
569 trial order to remove all significant associations. All neurons with coefficients larger than the 95th
570 percentile of the shuffled distribution (green shaded area in Fig. 6F) were considered to be correlated with
571 tectal activity. Across experiments, the proportion of MCNs exceeding this threshold varied (Fig. 6G) but
572 on average 30% (+/- 22% SD) of MCNs were positively correlated with tectal multisensory integration.

573

574 **Discussion**

575 This study provides the first comprehensive evidence of multisensory enhancement elicited by audiovisual
576 stimuli across neural and behavioral levels in zebrafish. Using visual and auditory danger cues, we
577 observed robust multisensory integration in the Tectum. We identified motion-correlated neurons in the
578 hindbrain which also show an increased response to multisensory stimulation. On a behavioral level,
579 multisensory stimulation significantly enhanced escape response probability. This paradigm enables an
580 examination of how multisensory processing at the neural level influences overt behavioral decisions that,
581 to date, has not been explored in zebrafish and remains relatively rare in the literature on other species.

582

583 *Auditory, visual and multisensory units in the zebrafish Tectum*

584 Work in zebrafish and other species suggests that deeper tectal layers receive non-visual sensory inputs
585 (Knudsen, 1982; Kardamakis et al., 2016; Vanwalleghem et al., 2017; Isa et al., 2021), supporting the role
586 of the Tectum as a multisensory integrative structure. Our findings contribute to this concept,
587 demonstrating that auditory information reaches the deeper layers of the zebrafish tectal neuropil. The
588 auditory response within these layers is robust and it is enhanced during multisensory stimulation (Fig. 4),
589 suggesting that integratory circuits that have been found in other vertebrates are anatomically conserved
590 in zebrafish.

591 We identified a significant presence of neurons in the Tectum that respond to multiple sensory modalities,
592 a finding documented in other species but scarcely observed in zebrafish. Previous reports using non-
593 threatening cues estimated that less than 1% of tectal cells were responsive to both visual and auditory
594 stimulation (Thompson et al., 2016). Here we found a much larger proportion of audiovisual-responsive
595 cells which averaged 19% across experiments (Fig. 3C-D). These audiovisual neurons were responsive to
596 unisensory stimuli, but exhibited increased activation probability under multisensory conditions (Fig. 3D),
597 suggesting that neurons that receive audiovisual inputs have a higher firing probability if those signals
598 arrive simultaneously.

599 We also found a proportion of tectal neurons that were only recruited when the auditory stimulus was
600 simultaneous with the end of the visual expansion and never responded to either visual or auditory stimuli
601 independently (EM neurons, Fig. 5B-E-F). It's important to note that these neurons are likely not
602 exclusively multisensory for all possible visual and auditory stimuli (i.e. stronger unisensory stimulation
603 might evoke responses in these units), but under our stimulation regime they only show suprathreshold

activity when both inputs are present. This finding parallels what is known about the superior colliculus in mammals, supporting a preserved functional role between these homologous brain structures (Stein & Stanford, 2008; Meredith & Stein, 1986). Previous reports on the zebrafish Tectum from Thompson et al. (2016) identified a suppression of visual responses when an auditory stimulus was presented simultaneously. In contrast, we did not find suppression but enhancement of visual responses when the auditory component was present (Fig. 4 and 5). One possible explanation for this discrepancy is the nature of the stimuli used in each study. Unlike Thompson et al., which used long pure tones intended to cover the larval hearing range, our study employed abrupt auditory stimuli specifically associated with aversive contexts (Fig. 1). The Tectum is known to differentiate between cues of varying ecological significance, such as prey and predator signals (Semmelhack et al., 2014; Temizer et al., 2015; Dunn et al., 2016). This may specifically enhance integration for aversive or appetitive stimuli, while neutral or mismatched cues may lead to multisensory suppression. Indeed, we found that when multisensory integration in the Tectum was suppressive, activity in MCN was minimum (Fig. 6E) suggesting that no motor response would be evoked. Further studies are needed to investigate the effect of stimulus valence in tectal multisensory integration.

About 20% of tectal neurons did not respond to any of our stimuli (Fig. 5B). This is unsurprising given the topographic organization of the Tectum and the spatially localized nature of our visual stimulus within the animal's visual field. However, previous studies in zebrafish (Thompson et al., 2016) indicate that certain neurons respond exclusively to non-audiovisual modalities. Specifically in zebrafish, tectal neurons known to be selectively responsive to water flow stimuli receive inputs from the lateral line nerve (Fame et al., 2006). Thus, lack of response in a subpopulation of neurons might be indicative of a modality not tested in our study.

Finally, it is noteworthy that we observed a pronounced inverse effectiveness pattern, particularly in the neuropil (Fig. 4E-F), where the dendrites of tectal neurons are located (Hiramoto & Cline, 2009; Baier & Scott, 2024). This anatomical arrangement suggests that subthreshold effects of dendritic integration could be most visible in this area compared to the somas in the PVL. The presence of inverse effectiveness in the zebrafish Tectum mirrors findings in the superior colliculus of mammals and the Tectum in other vertebrate models (Meredith & Stein, 1986; Stein et al., 2008; Gil-Guevara, Bernal, & Riveros, 2022; Sumby & Pollack, 1954), suggesting an evolutionary conserved multisensory integration mechanism.

A functional relationship between tectal integration and behavior

In this work, we introduce a methodology for extracting motor event data when simultaneously recording tail movements is not feasible. We demonstrated that these movement events are reliably evoked by both visual and auditory stimuli and show multisensory integration consistent with our behavioral findings (Fig. 6A). Additionally, we showed that, even with this inferred movement data, it is possible to identify neurons correlated with these motor events, including both spontaneous movements and stimulus-evoked responses (Fig. 6B-C). In freely moving and in agarose embedded fish, auditory stimuli evoked slightly higher response rates than visual stimuli (Fig. 1D and 6A). The fact that motion events of agarose-embedded fish were associated with the presentation of danger stimuli and that they exhibit multisensory

643 enhancement qualitatively similar to freely-swimming fish suggests that these events represent escape-
644 like attempts.

645 We report for the first time a relationship between the multisensory enhancement observed in the
646 Tectum and the activity of motion-correlated neurons in the hindbrain, which receive projections from
647 the Tectum (Del Bene et al., 2010; Robles et al., 2011; Kardamakis et al., 2016; Baier & Scott, 2024).
648 Hindbrain neurons drive premotor activity—for instance, prepontine neurons in rhombomere 1 are
649 implicated in evoking long latency C-starts (Marquart et al., 2019) or the Mauthner cells, in rhombomere
650 4, are responsible of the short latency C-start. Here we show that multisensory enhancement in the
651 Tectum correlates with an increase in the likelihood of premotor activity (Fig. 6-G). This, in turn, may
652 contribute to the behavioral enhancement we observe, both in agarose-embedded and freely moving
653 animals (Fig. 1), implying a causal link between tectal and behavioral multisensory enhancement.

654 Our work shows that the zebrafish Tectum integrates multisensory stimuli, producing both sublinear and
655 supralinear enhancement at the single-neuron level and at the population level. This multisensory activity
656 is closely related to the activation of functionally identifiable neurons in the hindbrain. Multisensory
657 integration increases the activity of these neurons and in turn enhances escape probability, particularly
658 when unisensory components are of low salience providing critical information for threat detection.

References

Baier, H., & Scott, E. K. (2024). The visual systems of zebrafish. Annual Review of Neuroscience, 47.

Barker, A. J., & Baier, H. (2015). Sensorimotor decision making in the zebrafish Tectum. Current Biology, 25(21), 2804–2814.

Bhattacharyya, K., McLean, D. L., & MacIver, M. A. (2017). Visual threat assessment and reticulospinal encoding of calibrated responses in larval zebrafish. Current Biology, 27(18), 2751–2762.

Burgess, H. A., & Granato, M. (2007). Sensorimotor gating in larval zebrafish. Journal of Neuroscience, 27(18), 4984–4994.

Del Bene, F., Wyart, C., Robles, E., Tran, A., Looger, L., Scott, E. K., ... & Baier, H. (2010). Filtering of visual information in the Tectum by an identified neural circuit. Science, 330(6004), 669–673.

Dunn, T. W., Gebhardt, C., Naumann, E. A., Riegler, C., Ahrens, M. B., Engert, F., & Del Bene, F. (2016). Neural circuits underlying visually evoked escapes in larval zebrafish. Neuron, 89(3), 613–628.

Fame, R. M., Brajon, C., & Ghysen, A. (2006). Second-order projection from the posterior lateral line in the early zebrafish brain. Neural Development, 1, 4.

Fleisch, V. C., & Neuhauss, S. C. (2006). Visual behavior in zebrafish. Zebrafish, 3(2), 191–201.

Foreman, M. B., & Eaton, R. C. (1993). The direction change concept for reticulospinal control of goldfish escape. Journal of Neuroscience, 13(10), 4101–4113.

Gabbiani, F., Krapp, H. G., Koch, C., & Laurent, G. (2002). Multiplicative computation in a visual neuron sensitive to looming. Nature, 420(6913), 320–324.

Ghosh, D. D., Nitabach, M. N., Zhang, Y., & Harris, G. (2017). Multisensory integration in C. elegans. Current Opinion in Neurobiology, 43, 110–118.

Gil-Guevara, O., Bernal, H. A., & Riveros, A. J. (2022). Honey bees respond to multimodal stimuli following the principle of inverse effectiveness. Journal of Experimental Biology, 225.

Giovannucci, A., Friedrich, J., Gunn, P., Kalfon, J., Brown, B. L., Koay, S. A., ... & Pnevmatikakis, E. A. (2019). CaImAn an open source tool for scalable calcium imaging data analysis. eLife, 8, e38173.

Hartline, P. H., Kass, L., & Loop, M. S. (1978). Merging of modalities in the optic Tectum: infrared and visual integration in rattlesnakes. Science, 199(4334), 1225–1229.

Hiramoto, M., & Cline, H. T. (2009). Convergence of multisensory inputs in Xenopus tadpole Tectum. Developmental Neurobiology, 69(14), 959–971.

Isa, T., Marquez-Legorreta, E., Grillner, S., & Scott, E. K. (2021). The Tectum/superior colliculus as the vertebrate solution for spatial sensory integration and action. Current Biology, 31(11), R741–R762.

690 Kalueff, A. V., Gebhardt, M., Stewart, A. M., Cachat, J. M., Brimmer, M., Chawla, J. S., ... & Schneider, and
691 the Zebrafish Neuroscience Research Consortium, H. (2013). Towards a comprehensive catalog of
692 zebrafish behavior 1.0 and beyond. Zebrafish, 10(1), 70–86.

693 Kardamakis, A. A., Perez-Fernandez, J., & Grillner, S. (2016). Spatiotemporal interplay between
694 multisensory excitation and recruited inhibition in the lamprey optic Tectum. eLife, 5, e16472.

695 Kimmel, C. B., Patterson, J., & Kimmel, R. O. (1974). The development and behavioral characteristics of
696 the startle response in the zebra fish. Developmental Psychobiology, 7(1), 47–60.

697 Knudsen, E. I. (1982). Auditory and visual maps of space in the optic Tectum of the owl. Journal of
698 Neuroscience, 2(9), 1177–1194.

699 Kohashi, T., & Oda, Y. (2008). Initiation of Mauthner-or non-Mauthner-mediated fast escape evoked by
700 different modes of sensory input. Journal of Neuroscience, 28(42), 10641–10653.

701 Liu, K. S., & Fetcho, J. R. (1999). Laser ablations reveal functional relationships of segmental hindbrain
702 neurons in zebrafish. Neuron, 23(2), 325–335.

703 Lukas, J., Romanczuk, P., Klenz, H, Klamser, P., Arias Rodriguez, L., Krause, J., & Bierbach, D. (2021).
704 Acoustic and visual stimuli combined promote stronger responses to aerial predation in fish. Behavioral
705 Ecology, 32(6), 1094–1102.

706 Luksch, H. (2009). Optic Tectum: Sensorimotor Integration. , 263–269.

707 Macaluso, E., & Driver, J. (2005). Multisensory spatial interactions: a window onto functional integration
708 in the human brain. Trends in Neurosciences, 28(5), 264–271.

709 Marques, J. C., Lackner, S., Félix, R., & Orger, M. B. (2018). Structure of the zebrafish locomotor
710 repertoire revealed with unsupervised behavioral clustering. Current Biology, 28(2), 181–195.

711 Marquart, G. D., Tabor, K. M., Bergeron, S. A., Briggman, K. L., & Burgess, H. A. (2019). Prepontine non-
712 giant neurons drive flexible escape behavior in zebrafish. PLOS Biology, 17(10), e3000480.

713 Marquez-Legorreta, E., Piber, M., & Scott, E. K. (2020). Visual escape in larval zebrafish: stimuli, circuits,
714 and behavior. In Behavioral and Neural Genetics of Zebrafish (pp. 49–71). Academic Press.

715 Martorell, N., & Medan, V. (2022). Audiovisual integration in the Mauthner cell enhances escape
716 probability and reduces response latency. Scientific Reports, 12(1), 1097.

717 Mathis, A., Mamidanna, P., Cury, K. M., Abe, T., Murthy, V. N., Mathis, M. W., & Bethge, M. (2018).
718 DeepLabCut: markerless pose estimation of user-defined body parts with deep learning. Nature
719 Neuroscience, 21(9), 1281–1289.

720 McIntyre, C., & Preuss, T. (2019). Influence of stimulus intensity on multimodal integration in the startle
721 escape system of goldfish. Frontiers in Neural Circuits, 13, 7.

722 Medan, V., & Preuss, T. (2014). The Mauthner-cell circuit of fish as a model system for startle plasticity.
723 Journal of Physiology–Paris, 108(2–3), 129–140.

724 Meredith, M. A., & Stein, B. E. (1986). Visual, auditory, and somatosensory convergence on cells in
725 superior colliculus results in multisensory integration. Journal of Neurophysiology, 56(3), 640–662.

726 Nevin, L. M., Robles, E., Baier, H., & Scott, E. K. (2010). Focusing on optic Tectum circuitry through the
727 lens of genetics. BMC Biology, 8, 1–10.

728 Ohyama, T., Schneider-Mizell, C. M., Fetter, R. D., Aleman, J. V., Franconville, R., Rivera-Alba, M., ... &
729 Zlatic, M. (2015). A multilevel multimodal circuit enhances action selection in Drosophila. Nature,
730 520(7549), 633–639.

731 Olcese, U., Iurilli, G., & Medini, P. (2013). Cellular and synaptic architecture of multisensory integration
732 in the mouse neocortex. Neuron, 79(3), 579–593.

733 Poulsen, R. E., Scholz, L. A., Constantin, L., Favre-Bulle, I., Vanwalleghem, G. C., & Scott, E. K. (2021).
734 Broad frequency sensitivity and complex neural coding in the larval zebrafish auditory system. Current
735 Biology, 31(9), 1977–1987.

736 Preuss, T., Osei-Bonsu, P. E., Weiss, S. A., Wang, C., & Faber, D. S. (2006). Neural representation of
737 object approach in a decision-making motor circuit. Journal of Neuroscience, 26(13), 3454–3464.

738 Privat, M., Romano, S. A., Pietri, T., Jouary, A., Boulanger-Weill, J., Elbaz, N., ... & Sumbre, G. (2019).
739 Sensorimotor transformations in the zebrafish auditory system. Current Biology, 29(23), 4010–4023.

740 Randlett, O., Wee, C. L., Naumann, E. A., Nnaemeka, O., Schoppik, D., Fitzgerald, J. E., ... & Schier, A. F.
741 (2015). Whole-brain activity mapping onto a zebrafish brain atlas. Nature Methods, 12(11), 1039–1046.

742 Robles, E., Smith, S. J., & Baier, H. (2011). Characterization of genetically targeted neuron types in the
743 zebrafish optic Tectum. Frontiers in Neural Circuits, 5, 1.

744 Rowland, B. A., Quessy, S., Stanford, T. R., & Stein, B. E. (2007). Multisensory integration shortens
745 physiological response latencies. Journal of Neuroscience, 27(22), 5879–5884.

746 Sajovic, P., & Levinthal, C. (1982). Visual cells of zebrafish optic Tectum: mapping with small spots.
747 Neuroscience, 7(10), 2407–2426.

748 Scott, E. K., & Baier, H. (2009). The cellular architecture of the larval zebrafish Tectum, as revealed by
749 gal4 enhancer trap lines. Frontiers in Neural Circuits, 3, 712.

750 Semmelhack, J. L., Donovan, J. C., Thiele, T. R., Kuehn, E., Laurell, E., & Baier, H. (2014). A dedicated
751 visual pathway for prey detection in larval zebrafish. eLife, 3, e04878.

752 Stanford, T. R., Quessy, S., & Stein, B. E. (2005). Evaluating the operations underlying multisensory
753 integration in the cat superior colliculus. Journal of Neuroscience, 25(28), 6499–6508.

754 Stein, B. E., & Stanford, T. R. (2008). Multisensory integration: current issues from the perspective of the
755 single neuron. Nature Reviews Neuroscience, 9(4), 255–266.

Stein, B. E., Stanford, T. R., Ramachandran, R., Perrault, T. J., Jr., & Rowland, B. A. (2009). Challenges in quantifying multisensory integration: alternative criteria, models, and inverse effectiveness. Experimental Brain Research, 198(2–3), 113–126.

Stevenson, R. A., Ghose, D., Fister, J. K., Sarko, D. K., Altieri, N. A., Nidiffer, A. R., ... & Wallace, M. T. (2014). Identifying and quantifying multisensory integration: a tutorial review. Brain Topography, 27, 707–730.

Sumby, W. H., & Pollack, I. (1954). Visual contribution to speech intelligibility in noise. The Journal of the Acoustical Society of America, 26(2), 212–215.

Temizer, I., Donovan, J. C., Baier, H., & Semmelhack, J. L. (2015). A visual pathway for looming-evoked escape in larval zebrafish. Current Biology, 25(14), 1823–1834.

Thompson, A. W., Vanwalleghem, G. C., Heap, L. A., & Scott, E. K. (2016). Functional profiles of visual-, auditory-, and water flow-responsive neurons in the zebrafish Tectum. Current Biology, 26(6), 743–754.

Van Atteveldt, N., Murray, M. M., Thut, G., & Schroeder, C. E. (2014). Multisensory integration: flexible use of general operations. Neuron, 81(6), 1240–1253.

Vanwalleghem, G., Heap, L. A., & Scott, E. K. (2017). A profile of auditory-responsive neurons in the larval zebrafish brain. Journal of Comparative Neurology, 525(14), 3031–3043.

Wallace, M. T., Meredith, M. A., & Stein, B. E. (1993). Converging influences from visual, auditory, and somatosensory cortices onto output neurons of the superior colliculus. Journal of Neurophysiology, 69(6), 1797–1809.

Whitchurch, E. A., & Takahashi, T. T. (2006). Combined auditory and visual stimuli facilitate head saccades in the barn owl (Tyto alba). Journal of Neurophysiology, 96(2), 730–745.

Zottoli, S. J. (1977). Correlation of the startle reflex and Mauthner cell auditory responses in unrestrained goldfish. Journal of Experimental Biology, 66(1), 243–254.

Zottoli, S. J., Hordes, A. R., & Faber, D. S. (1987). Localization of optic tectal input to the ventral dendrite of the goldfish Mauthner cell. Brain Research, 401(1), 113–121.

Zottoli, S. J., Newman, B. C., Rieff, H. I., & Winters, D. C. (1999). Decrease in occurrence of fast startle responses after selective Mauthner cell ablation in goldfish (Carassius auratus). Journal of Comparative Physiology A, 184, 207–218.

785 **FIGURES**

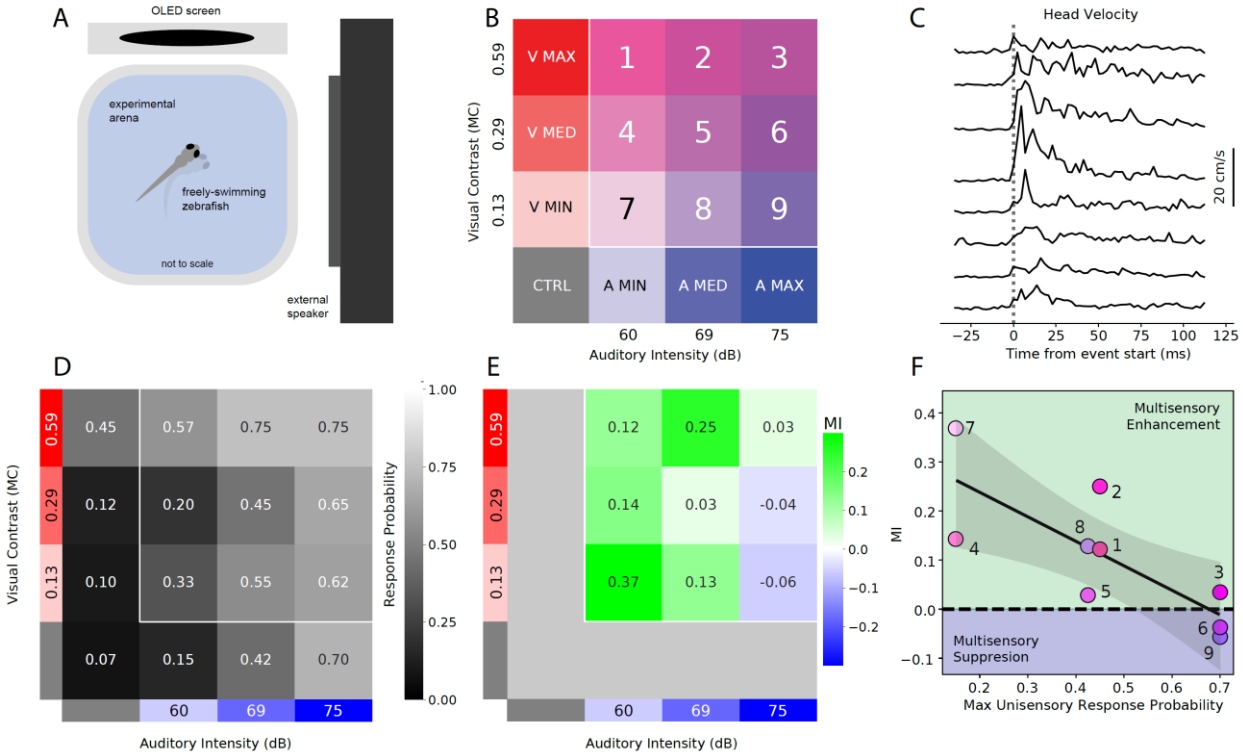

786

787 **Figure 1. Multisensory enhancement of escape probability is inversely related to stimulus intensity.** (A)
788 Experimental arena used to present visual and auditory stimuli to freely-swimming zebrafish (N = 80). (B) Stimulus
789 grid containing three visual contrasts (V min, V med, V max), three auditory intensities (A min, A med, A max), their
790 nine combinations (1-9) and a no-stimulus (Ctrl) condition. Multisensory stimuli are numbered to be used as
791 reference in Fig. 1F. MC: Michelson Contrast. (C) Eight representative examples of motor events. Fast events are
792 defined as those which surpass a threshold of 6 cm/s. Traces are aligned to the event's start time (vertical dotted
793 line). (D) Escape response probability for each unisensory stimulus and for each combination of visual and auditory
794 intensities (n = 40). (E) Multisensory Integration coefficient (MI) for each combination of visual and auditory
795 intensities. Color code indicates MI strength. (F) MI for each multisensory condition, as a function of maximum
796 unisensory response probability. Each point represents a single multisensory condition corresponding to a
797 combination in Fig. 1B, averaged across all fish. Black line represents a linear fit and its confidence interval.

798

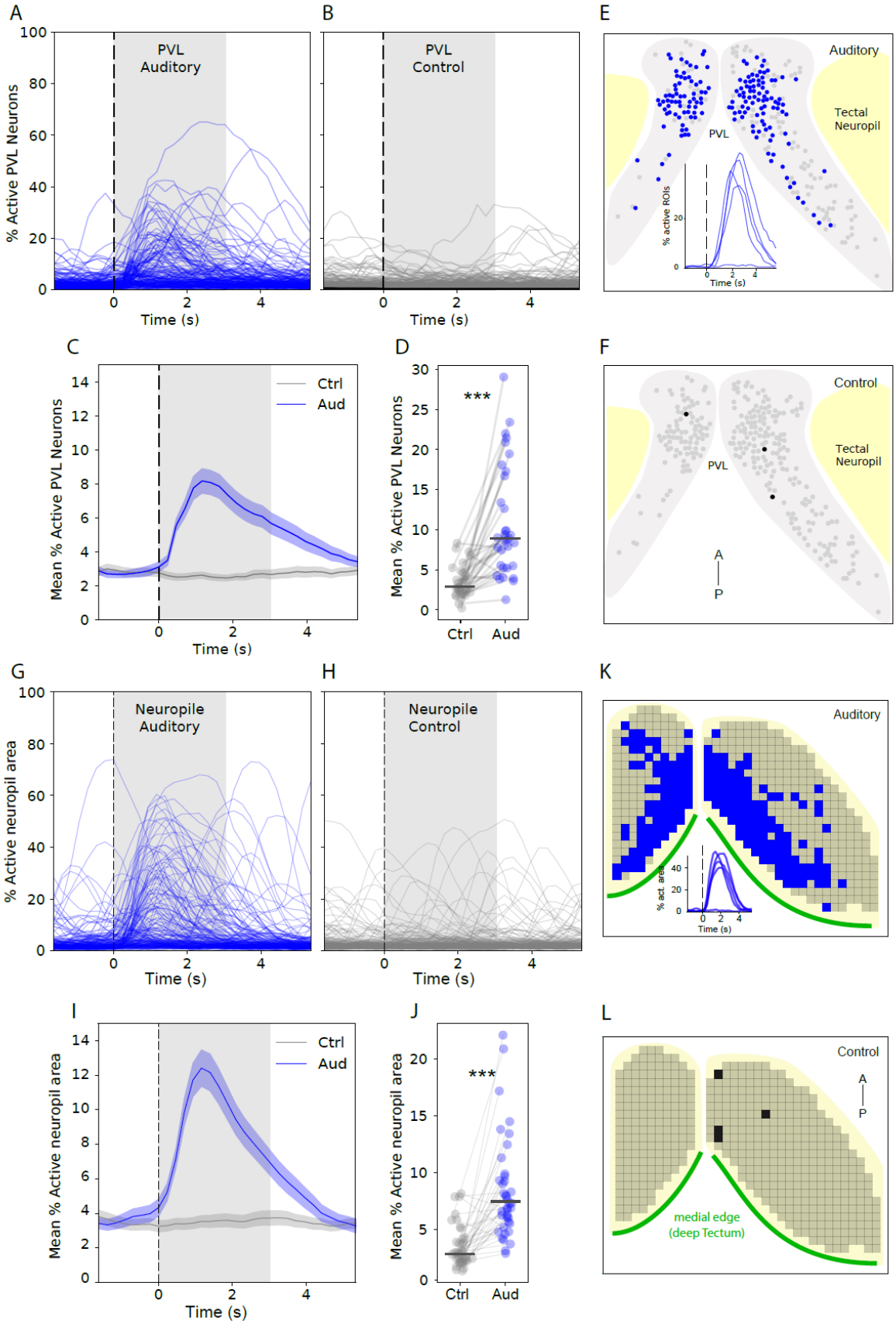
A
PVL
Auditory
% Active PVL Neurons
Time (s)
B
PVL
Control
Time (s)
E
Auditory
Tectal
Neuropil
PVL
% active ROIs
Time (s)
C
Ctrl
Aud
Mean % Active PVL Neurons
Time (s)
D
***
Mean % Active PVL Neurons
Ctrl
Aud
F
Control
Tectal
Neuropil
PVL
A
P
G
Neuropile
Auditory
% Active neuropil area
Time (s)
H
Neuropile
Control
Time (s)
K
Auditory
% act. area
Time (s)
I
Ctrl
Aud
Mean % Active neuropil area
Time (s)
J
***
Mean % Active neuropil area
Ctrl
Aud
L
Control
A
P
medial edge
(deep Tectum)

799

Figure 2. Auditory stimulation elicits neural responses in the Optic Tectum of zebrafish. (A) % of active PVL Neurons during auditory trials. Each line represents a trial. Auditory responses are analyzed over a 3-s period (shaded area) after sound presentation (vertical dashed line, 5 trials per animal, n = 33). (B) Same as A for control trials (no stimulation, 5 trials per animal, N = 33). (C) Mean (+/- SE) proportion of active ROIs in the PVL over time as a response to auditory (blue) and control (gray) trials, across experiments. (D) Mean proportion of active ROIs in the PVL after stimulation (shaded period in A-B) in auditory and control trials for each experiment. Connected data points correspond to single experiments, averaged across 5 trials for each condition. ***$p<0.001$. (E) Distribution of active PVL ROIs (blue dots) during the analysis window (3.5 s after end of stimulus presentation) for a representative example. % of active ROIs for each trial of the depicted example is shown in the inset. PVL is outlined in grey while the yellow area represents the neuropile. (F) Distribution of active PVL ROIs (black dots) during control trials of the same experiment as in E. (G) Auditory stimuli increase the proportion of active tectal neuropil area, compared to spontaneous activation (H) (5 trials per animal, n = 33). Inset shows neuropil regions which were activated in at least one trial for the illustrated example. (I) Mean proportion of active neuropil area over time as a response to auditory (blue) and control (gray) trials, across experiments. (J) Proportion of active neuropil area during the stimulus window in control and auditory trials, for each experiment. Connected data points correspond to single experiments, averaged across 5 trials for each condition. ***$p<0.001$. (K) Distribution of active neuropile area (blue squares) during the analysis window (3.5 s after end of stimulus presentation) for a representative example. % of active area for each trial of the depicted example is shown in the inset. (L) Distribution of active neuropile area during control trials of the same experiment as in K. Green curves show the medial edge of the tectal neuropils, corresponding to deeper layers of the Tectum.

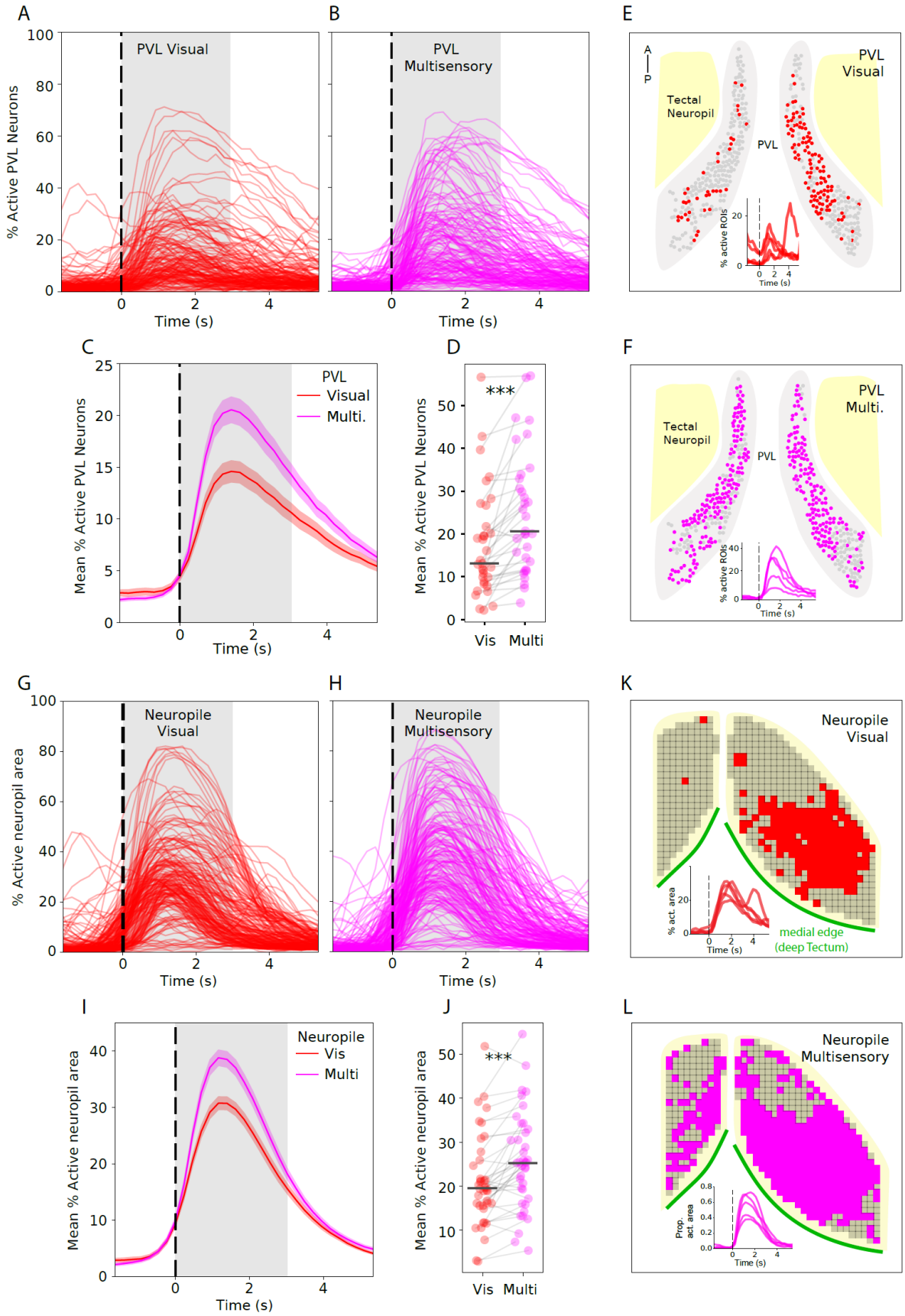
A
PVL Visual
% Active PVL Neurons
Time (s)
B
PVL Multisensory
Time (s)
E
A
P
Tectal Neuropil
PVL
PVL Visual
% active ROIs
Time (s)
C
PVL
Visual
Multi.
Mean % Active PVL Neurons
Time (s)
D
***
Mean % Active PVL Neurons
Vis
Multi
F
Tectal Neuropil
PVL
PVL Multi.
% active ROIs
Time (s)
G
Neuropile Visual
% Active neuropil area
Time (s)
H
Neuropile Multisensory
Time (s)
K
Neuropile Visual
% act. area
Time (s)
medial edge
(deep Tectum)
I
Neuropile
Vis
Multi
Mean % Active neuropil area
Time (s)
J
***
Mean % Active neuropil area
Vis
Multi
L
Neuropile Multisensory
Prop. act. area
Time (s)

821

822 **Figure 3. Multisensory stimulation enhances neural responses over a unisensory visual stimulus in the Tectum of**
823 **zebrafish.** (A) % of active PVL Neurons during visual trials. Each line represents a trial (5 trials per animal, n = 33).
824 The vertical dashed line represents the end of the visual loom expansion (B) Multisensory trials (5 trials per animal,
825 n = 33) show significant activation after the stimulus presentation (vertical dashed line: sound presentation
826 concurrent with end of looming expansion). (C) Mean proportion of active ROIs in the PVL over time as a response
827 to multisensory (magenta) and visual (red) trials, across experiments. (D) Mean (+/- SE) proportion of active ROIs in
828 the PVL after stimulation time (shaded window in A-B) in visual and multisensory trials for each experiment. Pairs of
829 points correspond to single experiments, averaged across 5 trials for each condition. ***p<0.001. (E) Distribution of
830 active PVL ROIs (red dots) during the analysis window (3.5 s after end of visual presentation) for a representative
831 example. % of active ROIs for each trial of the depicted example is shown in the inset. (F) Distribution of active PVL
832 ROIs (magenta dots) during multisensory trials of the same experiment as in E showed a more distributed and
833 bilateral activation. % of active ROIs for each trial of the depicted example is shown in the inset. (G) Visually-evoked
834 activity in the neuropile. (H) Multisensory trials evoke a significant activation of the neuropile. (I) Mean (+/- SE)
835 proportion of active neuropil area over time as a response to visual (red) and multisensory (H, magenta) trials, across
836 experiments. (J) Mean proportion of active neuropil area during the stimulus window in visual and multisensory
837 trials for each experiment. Pairs of points correspond to single experiments, averaged across 5 trials for each
838 condition. ***p<0.001. (K) Distribution of active neuropile area (red squares) during the analysis window (3.5 s after
839 end of visual stimulus) for a representative example. % of active area for each trial of the depicted example is shown
840 in the inset. (L) Distribution of active neuropile area during multisensory trials of the same experiment as in K. Green
841 curves show the medial edge of the tectal neuropile.

842

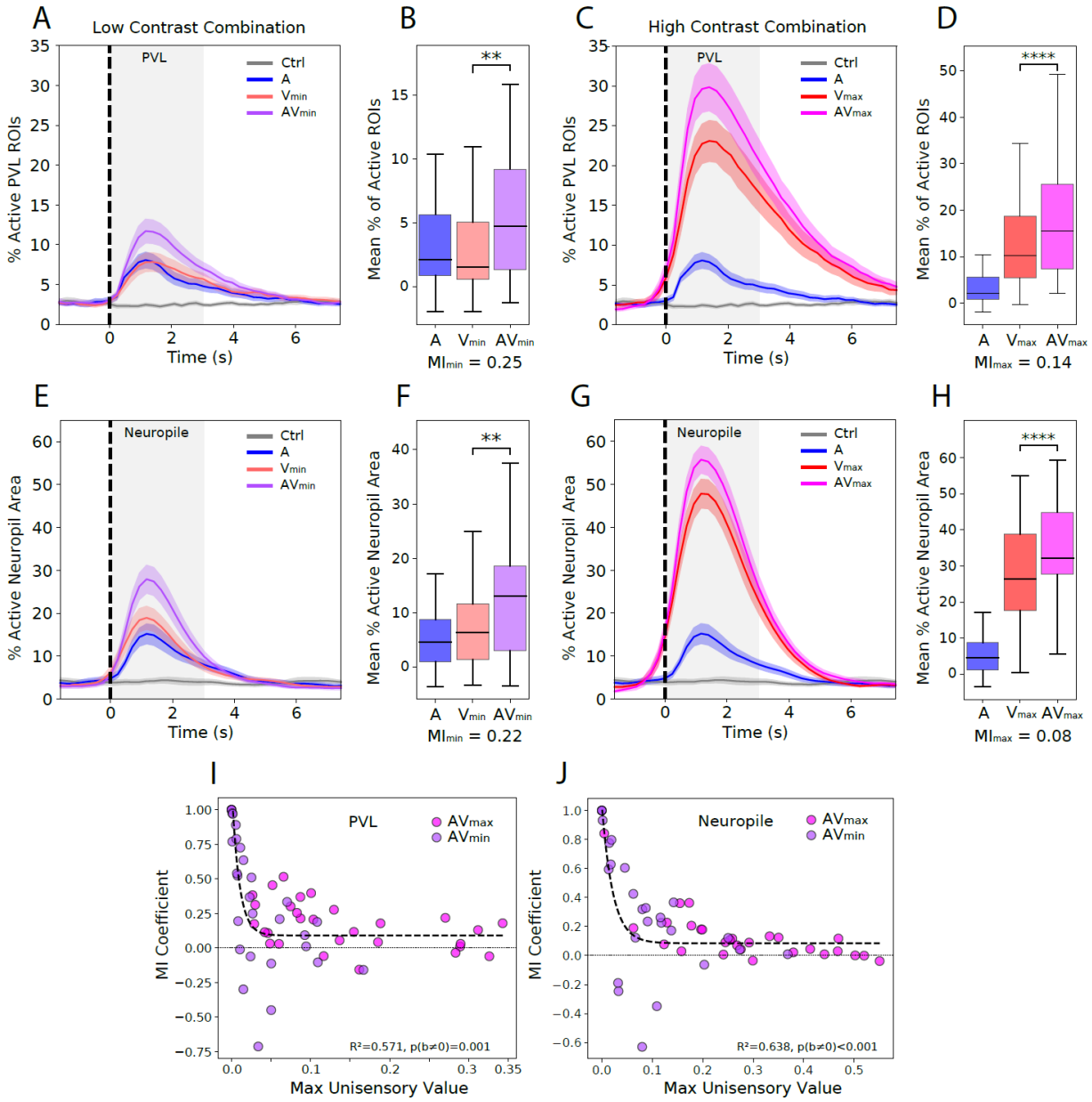

Figure 4. Inverse effectiveness in the zebrafish Tectum. (A) Mean proportion of active ROIs over time in response to control (grey), auditory (blue), weak visual (V_{low}, light red) and multisensory (AV_{low}, purple) stimuli. (B) Mean proportion of active ROIs during the stimulation window subtracted from the control. **p=0.004. (C) Mean proportion of active ROIs over time in the PVL as a response to control (grey), auditory (blue), V_{high} (red) and multisensory (AV_{high}, magenta) stimuli. (D) Mean proportion of active ROIs during the stimulation window subtracted from the control. ***p<0.001. (E-F) Same as A-B for the neuropile. (G-H) Same as C-D for the neuropile. (I) MI in the PVL plotted against the maximum unisensory activation probability, for each experiment's low contrast (AV_{low}, purple) and high contrast multisensory stimulus (AV_{high}, magenta). Linear regression was performed on each subset (dashed purple and magenta lines). (J) Same as I for the neuropile.

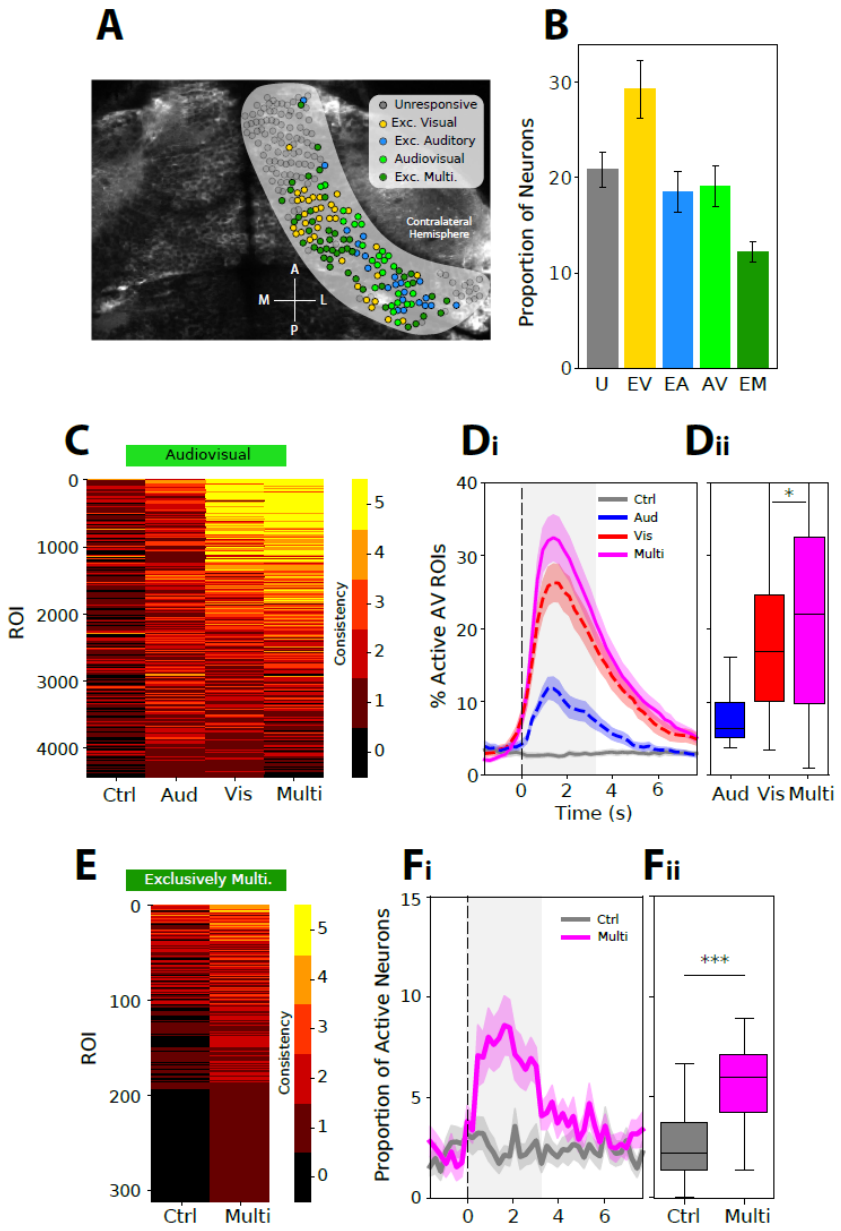

Figure 5. Multisensory stimulation recruits unresponsive PVL neurons and boosts response probability of audiovisual neurons. (A) Representative example of a PVL's neurons colored according to their response profile for the hemitectum contralateral to the visual stimulus. ROIs are overlaid on top of the template used for anatomical segmentation. (B) Proportion of neurons in each of the five neuron classes across experiments (mean +/- SD: U: 21 +/- 2, EA: 19 +/- 2, EV: 29 +/- 3, AV: 19 +/- 2, EM: 12 +/- 1). (C) Response consistency for all AV ROIs, for the control, auditory, visual and multisensory conditions. ROIs are sorted by their mean consistency across stimuli. (Di) Mean (+/- SE) proportion of active AV ROIs over time for each stimulation condition. (Dii) Mean peak proportion of active AV ROIs for auditory, visual and multisensory trials. *p = 0.012. (E) Response consistency for all EM ROIs, for the control and multisensory conditions. ROIs are sorted by their mean consistency across stimuli. (Fi) Mean (+/- SE) proportion of active EM ROIs over time for each stimulation condition. (Fii) Mean peak proportion of active EM ROIs for control and multisensory trials. ***p<0.001.

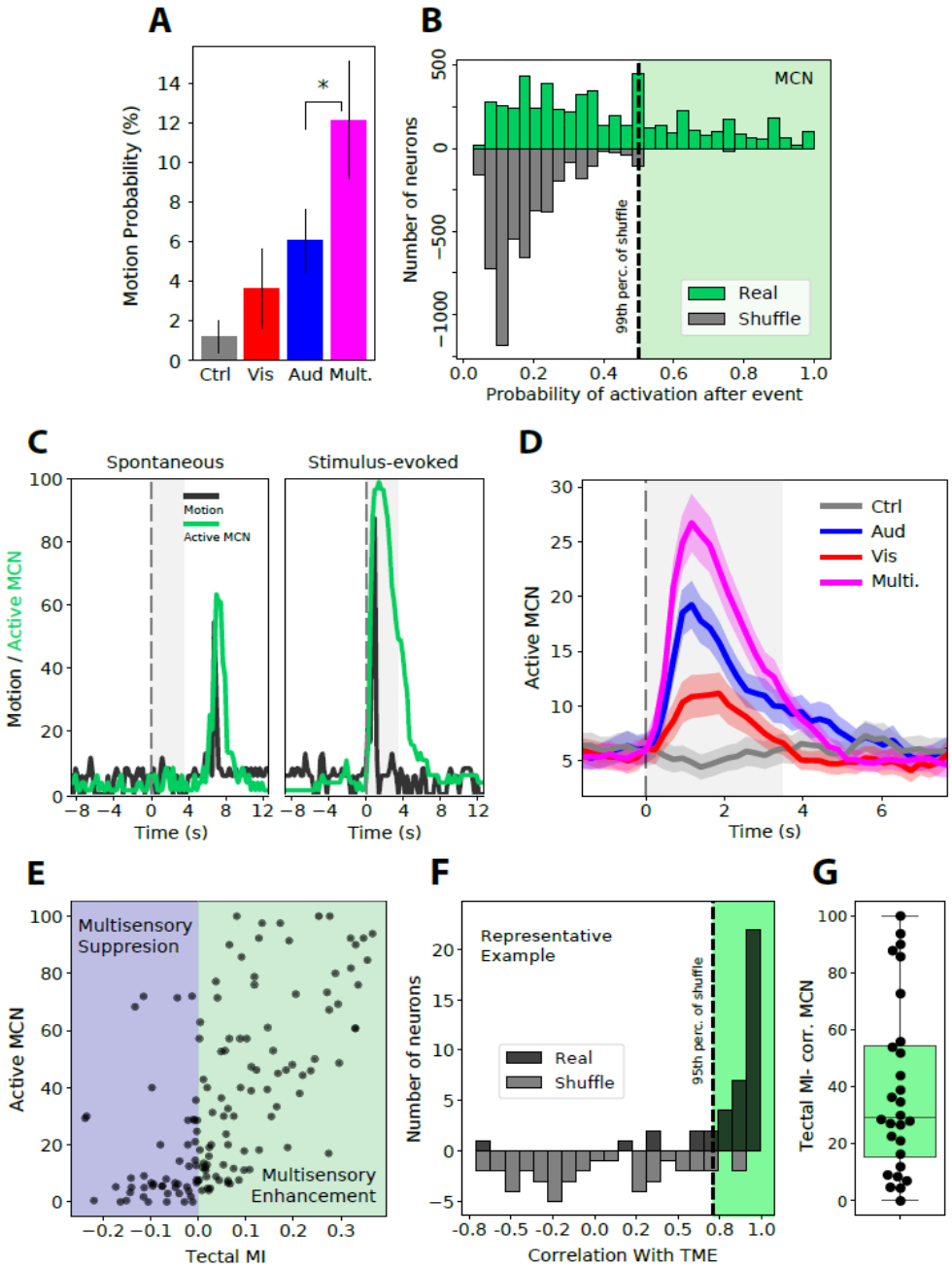

Figure 6. Motion-correlated neurons in the Hindbrain are mostly responsive to multisensory stimulation when tectal activity shows multisensory enhancement. (A) Motion event probability for each stimulation condition. Bars represent the mean motion probability across all experiments. *p = 0.029. (B) Distribution of the activation probability after a motion event, for all recorded Hindbrain neurons across experiments, computed for real events (green) or when shuffling times (gray). Only events outside the stimulation window were considered, to avoid biasing this analysis with the response to stimulation. Vertical dashed line represents 99th percentile of shuffle distribution. (C) The synchronous activation of motion-correlated neurons in the Hindbrain is highly indicative of spontaneous and stimulus-evoked motion events. Left: representative example of a spontaneous event (occurring outside the stimulation window). The black trace shows the displacement of the image acquired by the confocal microscope

(arbitrary units), while the green trace shows the proportion of active motion neurons in the Hindbrain. Right: Representative example of a stimulus-evoked event (occurring shortly after stimulus presentation). (D) Mean proportion of active MCNs over time, across all experiments, as a response to control, auditory, visual or multisensory stimuli. (E) Activation of MCNs in the Hindbrain as a function of Tectal MI. Each black dot represents a trial. Progressively stronger multisensory enhancement in the Tectum correlates with a higher proportion of active MCN. (F) A proportion of MCNs in the Hindbrain are associated with Tectal MI. Correlation between dF/F and Tectal MI for each MCN, for each of the 5 multisensory trials in a representative experiment. Black bars represent the distribution of correlation coefficients, while gray bars show the results of shuffling trial order to remove all significant associations. Vertical dashed line represents 95th percentile of shuffle distribution. Green-shaded region shows neurons with correlation coefficients in the top 5% of what would be expected by chance. (G) Proportion of MCNs whose dF/F was significantly correlated with Tectal MI across multisensory trials. Each datapoint is a single experiment.

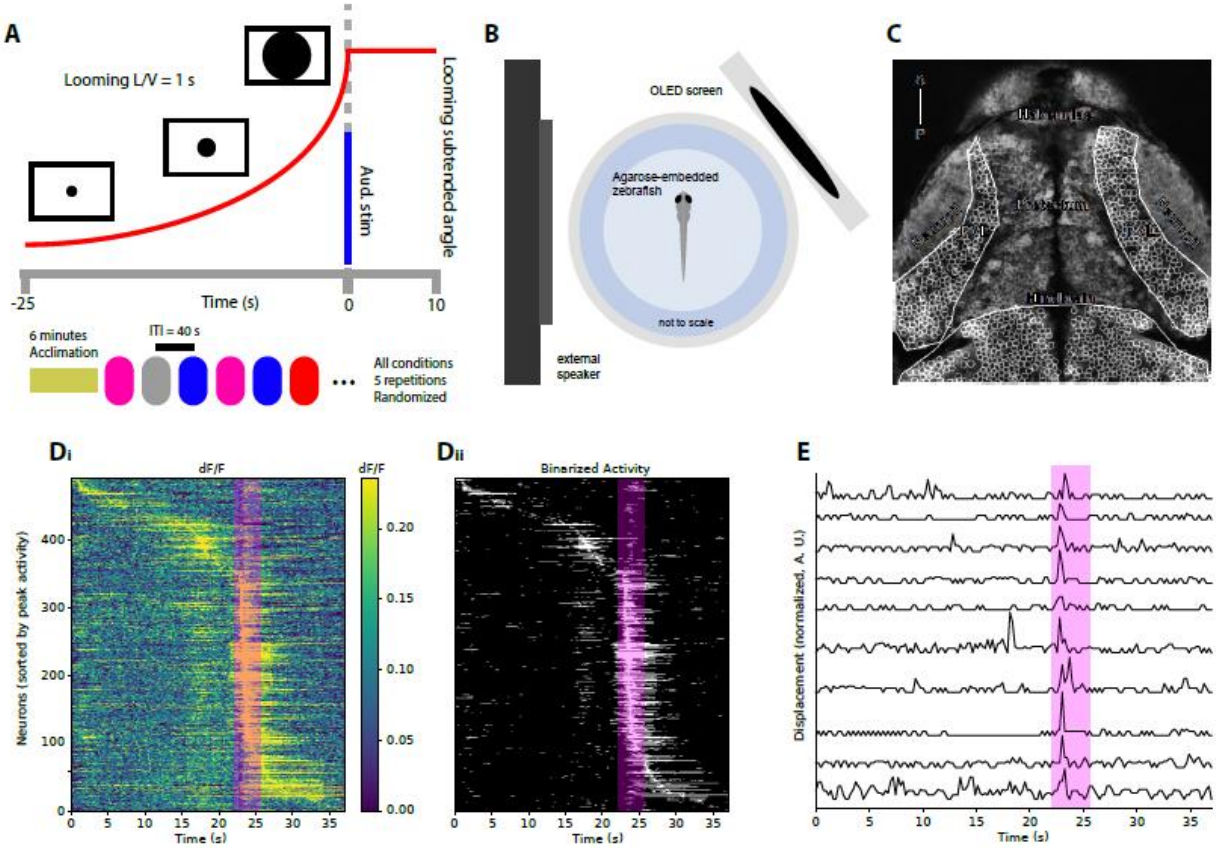

Supplementary Figure 1. Visual and auditory stimuli evoke tectal activity and motor events in agarose-embedded fish. (A) Experimental procedure and stimulus coordination (see Methods). (B) Setup diagram for imaging experiments. (C) Representative example of ROI segmentation. Visually-defined polygons for the Hindbrain and PVL are shown, with semi-automatic segmentation of circular ROIs inside each polygon. Tectal neuropil was not segmented using this method, but subdivided in a grid pattern. ROIs located outside selected polygons were ignored, as were ROIs which were never observed to be active. Hindbrain, PreTectum and Habenulae are labeled for reference. (D) Representative example of neural activity. (D_i) Individual traces of dF/F for each PVL ROI (n = 491) during a multisensory trial, sorted from top to bottom by time of peak activity. The region shaded in magenta represents the time window used to define neural response to stimulation. (D_{ii}) Binarized dF/F, as described in Methods, is shown for each PVL ROI during the same multisensory trial. (E) Ten representative examples of image displacement traces, captured by a motion-correction algorithm as described in Methods, in trials where a motion event was detected during the stimulation window (magenta shading).

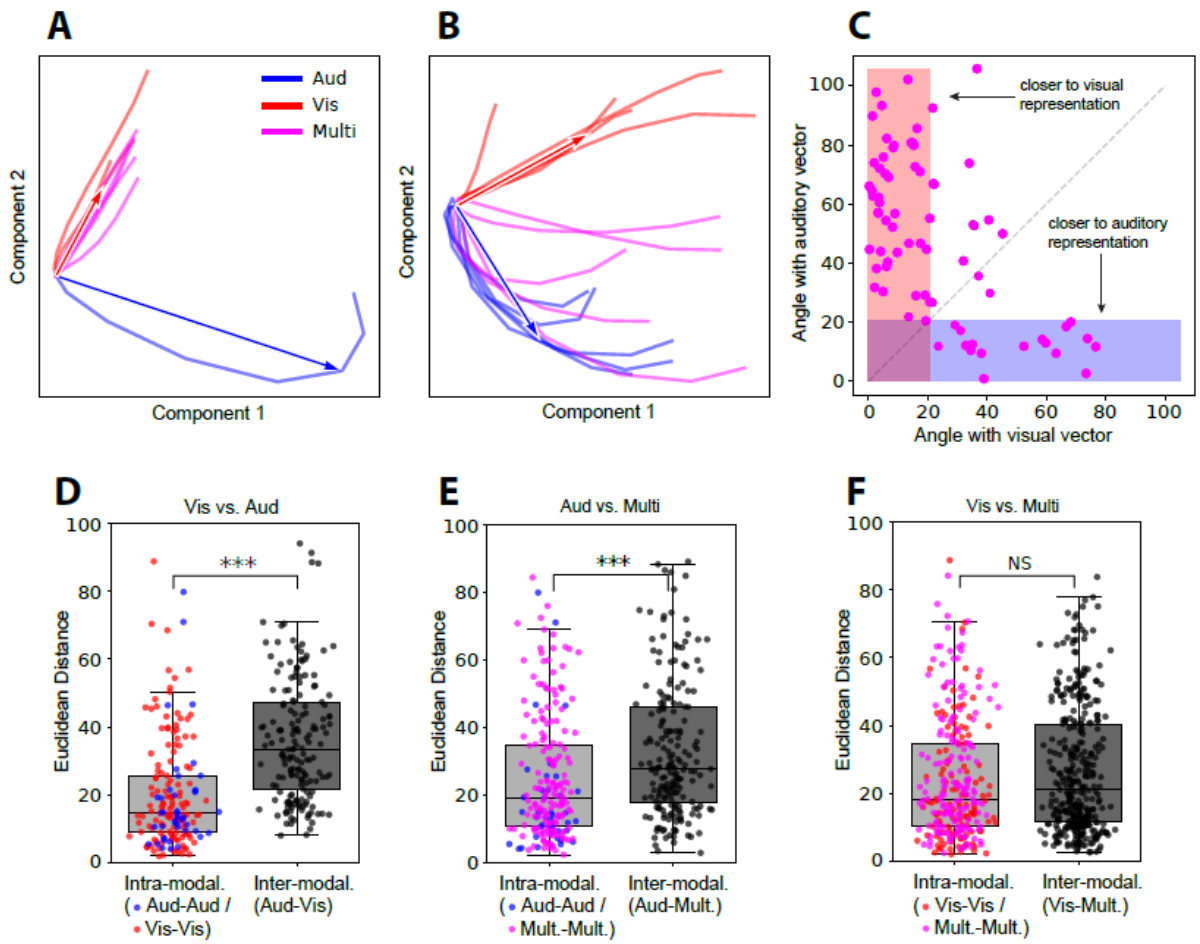

Supplementary Figure 2. Multisensory representation in the tectal PVL usually aligns closely to a single unisensory representation. (A-B) Representative examples of tPCA results for two different experiments. Trajectories of visual (red), auditory (blue), and multisensory (magenta) trials in the space defined by the first two principal components, in the 1.86 seconds after stimulation time, for each representative experiment. Arrows represent the median direction of visual and auditory trajectories. (C) Angle between each multisensory trajectory and the visual (x axis) and auditory (y axis) median directions for its corresponding experiment. Each point represents a single multisensory trial. The gray dashed line represents equal distance to both representations. (D) Euclidean distance between response trajectories of the same unisensory stimulus (Intra-modal, visual vs. visual, red, or auditory vs. auditory, blue) or between unisensory stimuli (Inter-modal., auditory vs. visual, black). Dots represent distances between individual trajectories compared to all other trajectories of the target class within an experiment. Boxplots represent the means of Intra-modality and Intermodality distances. ***$p<0.001$. (E) Same as D between response trajectories of the multisensory stimulus and auditory stimulus. ***$p<0.001$. (F) Same as D between response trajectories of the multisensory stimulus and visual stimulus. NS: statistically not significant.

Variable	Mean	Max	Min	Range	Feature Count
Head Velocity	x	x			2
End-Tail Velocity	x	x			2
Angular Velocity	x	x			2
Sum of Tail Angles	x	x		x	3
Mid-Tail Velocity	x	x			2
Head-Tail Distance	x		x		2
Head Acceleration	x	x		x	3
End-Tail Acceleration	x	x		x	3
Angular Acceleration	x	x		x	3
Head Jerk	x	x		x	3
End-Tail Jerk	x	x		x	3
Sum of Curvature	x	x		x	3
Angle Velocity Heading	x	x			2
Curvature Rate	x	x		x	3
Total					**36**

Supplementary Table 1: Kinematic descriptors of escape behaviors extracted from pose estimation data. Head Velocity: instantaneous speed of the head, calculated as the displacement of the midpoint between both eyes over time. End-Tail Velocity: instantaneous speed of the tail, derived from the movement of the mean point between the last two tail segments. Angular Velocity: rate of rotational change in the direction of the head, calculated from the angle between vectors connecting the head to a reference body point. Sum of Tail Angles: cumulative angular deviation between consecutive segments along the tail. Mid-Tail Velocity: instantaneous speed of the sixth tail segment, calculated from its displacement over time. Head-Tail Distance: linear distance between the head midpoint and the mean point of the tail's last segments. Head Acceleration: rate of change of the head's velocity. Tail Acceleration: rate of change of the tail's velocity. Angular Acceleration: rate of change in angular velocity. Head Jerk: rate of change of head acceleration. End-Tail Jerk: rate of change of tail acceleration. Sum of Curvature: cumulative discrete triangular curvature of the tail segments. Angle Velocity Heading: angle between the head's velocity vector and a reference vector from the head toward the body, indicating directional alignment of motion. Curvature Rate: rate of change of tail curvature over time. Note that from each of these parameters the Mean, Maximum, Minimum and/or Range was computed as individual variables used in the dimensionality reduction analysis.